Uncertainty Quantification for Low-Frequency, Time-Harmonic Maxwell Equations with Stochastic Conductivity Models

Uncertainty quantification for low-frequency, time-harmonic Maxwell equations with stochastic conductivity models

Dimitris Kamilis* and Nick Polydorides

Abstract. We consider an Uncertainty Quantification (UQ) problem for the low-frequency, time-harmonic Maxwell equations with conductivity that is modelled by a fixed layer and a lognormal random field layer. We formulate and prove the well-posedness of the stochastic and the parametric problem; the latter obtained using a Karhunen-Loève expansion for the random field with covariance function belonging to the anisotropic Whittle-Matérn class. For the approximation of the infinite-dimensional integrals in the forward UQ problem, we employ the Sparse Quadrature (SQ) method and we prove dimension-independent convergence rates for this model. These rates depend on the sparsity of the parametric representation for the random field and can exceed the convergence rate of the Monte-Carlo method, thus enabling a computationally tractable calculation for Quantities of Interest. To further reduce the computational cost involved in large-scale models, such as those occurring in the Controlled-Source Electromagnetic Method, this work proposes a combined SQ and model reduction approach using the Reduced Basis (RB) and Empirical Interpolation (EIM) methods. We develop goal-oriented, primal-dual based, a posteriori error estimators that enable an adaptive, greedy construction of the reduced problem using training sets that are selected from a sparse grid algorithm. The performance of the SQ algorithm is tested numerically and shown to agree with the estimates. We also give numerical evidence for the combined SQ-EIM-RB method that suggests a similar convergence rate. Finally, we report numerical results that exhibit the behaviour of quantities in the algorithm.

Key words. maxwell equations, uncertainty quantification, sparse quadrature, high-dimensional approximation, reduced basis method, empirical interpolation, computational electromagnetism

AMS subject classifications. 35R60, 35Q61, 62M40, 65N30, 65D30

1. Introduction.

Uncertainty Quantification (UQ) has been applied to a number of problems with the purpose of identifying and quantifying the uncertainty in the input and output of models [66, 67]. In the framework of probabilistic characterization of the uncertainty, the objective is the estimation of statistical Quantities of Interest (QoIs). When the model consists of a partial differential equation (PDE), UQ analysis proceeds using stochastic PDEs with the input and output described as random fields [1, 51]. Methods for the forward solution and statistical analysis of these stochastic PDEs are reviewed in [41] and include the Monte Carlo method and its variants [34, 38, 39, 40, 61], the stochastic collocation [70, 4, 68] and stochastic Galerkin [37, 71, 5] methods.

A general methodology is to reformulate the stochastic problem into a deterministic, countably parametric form with distributed uncertainty, leading to a high or infinite-dimensional integration problem for the statistical characterization of the input and outputs. Attempts to approximate these integrals are then faced with the challenge of achieving low computational costs and fast convergence rates that are affected as little as possible by the curse of high dimensionality. An approach that can be competitive in this regard, is high-dimensional

*Institute for Digital Communications, University of Edinburgh, U.K. (d.kamilis@ed.ac.uk, n.polydorides@ed.ac.uk)

polynomial approximation of parametric PDEs, which has been analysed in a number of publications [28, 27, 26, 6, 24, 25, 29]. The theoretical results show that sparsity or summability in the parametric representation of the input translates into sparse polynomial approximations for the output that converge with dimension-independent rates which depend on the level of sparsity in the input. In practice, one way to construct polynomial approximations is via interpolation, using evaluations at suitable deterministic sparse grid points [14]. This approach can be considered as equivalent to the stochastic collocation method. Additionally, as is known, interpolation gives rise to corresponding quadrature schemes, so sparse polynomial approximation via interpolation leads to Sparse Quadrature (SQ) [65, 63, 62], effectively discretising the integrals while inheriting the favourable convergence properties. The sparse grids can be constructed using a priori knowledge of the dependence of the output on the parametric dimensions or using heuristic dimension-adaptive algorithms [36, 62, 17].

An alternative approximation approach for parametric PDEs is the Reduced Basis (RB) model reduction method [59, 57, 11], which has been applied to electromagnetism in [46] for the electric field integral equation, in [10] for the time-dependent case and in [23, 49, 43] for the time-harmonic Maxwell equations. By using greedy algorithms with appropriate error estimators, RB methods enable the progressive approximation of parametric PDEs with controlled levels of accuracy and computational cost. Therefore, a promising approach is the combination of RB model reduction and of dimension-adaptive SQ schemes for the estimation of the pertinent integrals as suggested in [18] in the forward UQ context and in [21] for the Bayesian inverse problem. In the case of non-affine parametric PDEs, an additional approximation step is usually performed by the Empirical Interpolation Method (EIM) [9] to achieve an affine-parametric form [22].

The work in this paper is based on this approach as applied to the low-frequency, time-harmonic Maxwell equations with uncertain conductivity coefficient. We specifically consider models consisting of a deterministic and a stochastic conductivity layer; the latter represented as a lognormal random field with specified covariance function. Our analysis of SQ convergence for these models reveals the attainability of dimension-independent convergence rates under suitable assumptions. The proposed methodology is a modification of the aforementioned, combined, SQ-EIM-RB approach to the lognormal case, taking *explicitly* into account the underlying Gaussian measure. We mention also a number of other novelties in this paper, including the rigorous treatment of point sources and measurements through regularization, the use of anisotropic covariance functions and the derivation of a posteriori error estimators for the SQ-EIM-RB method. We note that a combination of Smolyak sparse grid stochastic collocation and Proper Orthogonal Decomposition model reduction for the time-harmonic Maxwell equations has been examined in [12], but the uncertainty there is in terms of a finite set of random variables representing material parameters in geometrical regions.

By studying this problem, we have in mind applications such as the Controlled Source Electromagnetic Method (CSEM) [30] which is a geophysical exploration method that aims to image the unknown sub-seabed conductivity from electric field measurements within the sea. While the objective there is the solution of the inverse problem, the UQ analysis we perform in this paper aims at understanding the influence of conductivity uncertainties in relevant models. Additionally, the approach and computational method are transferable to the more challenging Bayesian inverse problem with possible complications, see e.g. [64]), which we will

address in future work.

2. Model specification. In this section, we specify the physical and mathematical model of the problem under study by describing the deterministic, the stochastic and the parametric, deterministic models.

2.1. Notation. We denote by $D \subset \mathbb{R}^3$ a bounded, Lipschitz, polyhedral domain with connected boundary ∂D, by $\boldsymbol{n}$ the outward normal unit vector and by $\|\cdot\|_2$ the Euclidean norm. The function space of infinitely differentiable functions with compact support in D is denoted by $C_0^\infty(D)$. For a measure space (X, Σ, γ), with measure γ, we denote by $L^p(X, Y)$ the space of Σ-measurable functions $u : X \to Y$ with norm

$$\|u\|_{L^p(X,Y)} = \left(\int_X \|u(x)\|_Y^p \, d\gamma(x) \right)^{1/p} = \mathbb{E}\left[\|u\|_Y^p \right]^{1/p}, \tag{2.1}$$

when $1 \leq p < \infty$ and norm

$$\|u\|_{L^\infty(X,Y)} = \operatorname*{ess\,sup}_{x \in X} \|u(x)\|_Y, \tag{2.2}$$

when $p = \infty$, where $\|\cdot\|_Y$ is the norm of a separable Banach space Y.

When $X = \Theta$ is a sample space and $\gamma = \mathbb{P}$ is a probability measure, we get the Bochner space of p-integrable random variables $u : \Theta \to Y$, that take values in Y, denoted by $L^p(\Theta, Y)$. When $X = D$, $Y = \mathbb{C}$, Σ is the Borel σ-algebra and γ is the Lebesgue measure, we get the standard $L^p(D)$ spaces. In particular, for $p = 2$ we have the Hilbert space of square-integrable functions $L^2(D)$ with inner product $(u, v)_{L^2(D)} = \int_D u\overline{v} \, d\boldsymbol{x}$ where $\overline{v}$ is the complex conjugate of v. We will also need the Sobolev spaces

$$H^k(D) = W^{k,2}(D) = \{u \in L^2(D) : \partial^{\boldsymbol{\alpha}} u \in L^2(D) \quad \forall\, |\boldsymbol{\alpha}| < k\}, \tag{2.3}$$

$$W^{k,\infty}(D) = \{u \in L^\infty(D) : \partial^{\boldsymbol{\alpha}} u \in L^\infty(D) \quad \forall\, |\boldsymbol{\alpha}| < k\}, \tag{2.4}$$

where $\partial^{\boldsymbol{\alpha}} u = \partial^{|\boldsymbol{\alpha}|} u / \partial x_1^{a_1} \partial x_2^{a_2} \partial x_3^{a_3}$. For vector-valued functions, we analogously use the spaces $C_0^\infty(D, \mathbb{C}^3)$, $L^p(D, \mathbb{C}^3)$ and $H^k(D, \mathbb{C}^3)$. The space of square-integrable vectors that also have a square-integrable curl is defined by

$$H(\mathrm{curl}, D) = \{\boldsymbol{u} \in L^2(D, \mathbb{C}^3) : \nabla \times \boldsymbol{u} \in L^2(D, \mathbb{C}^3)\}, \tag{2.5}$$

with norm

$$\|\boldsymbol{u}\|_{H(\mathrm{curl},D)} = \left(\|\boldsymbol{u}\|_{L^2(D,\mathbb{C}^3)}^2 + \|\nabla \times \boldsymbol{u}\|_{L^2(D,\mathbb{C}^3)}^2 \right)^{1/2}. \tag{2.6}$$

The subspace $H_0(\mathrm{curl}, D)$ of functions $\boldsymbol{u} \in H(\mathrm{curl}, D)$, with vanishing tangential trace on the boundary ∂D, is defined as the completion of $C_0^\infty(D, \mathbb{C}^3)$ in the $H(\mathrm{curl}, D)$ norm.

We also make use of multi-index notation. Define by $\mathcal{F}$ the countable index set of all sequences $\boldsymbol{\nu} = (\nu_j)_{j \geq 1}$ of non-negative integers which are finitely supported (i.e. with a finite number of non-zero elements). For $\boldsymbol{\nu}, \boldsymbol{\mu} \in \mathcal{F}$ we use

$$|\boldsymbol{\nu}| = \sum_{j \geq 1} \nu_j < \infty, \quad \boldsymbol{\nu}! = \prod_{j \geq 1} \nu_j!, \quad \binom{\boldsymbol{\nu}}{\boldsymbol{\mu}} = \prod_{j \geq 1} \binom{\nu_j}{\mu_j}, \tag{2.7}$$

with $\binom{n}{m} = 0$ if $m > n$. By $\boldsymbol{\mu} \leq \boldsymbol{\nu}$ we denote the ordering $\mu_j \leq \nu_j$ for all j. The cardinality of an index set $\Lambda \subset \mathcal{F}$ is denoted by $\#(\Lambda)$ and the support of a sequence $\boldsymbol{\nu}$ is denoted by $\operatorname{supp}(\boldsymbol{\nu}) = \{j : \nu_j \neq 0\}$.

2.2. Deterministic model. We are interested in low-frequency electromagnetic models, such as the ones occurring in CSEM, which can be modelled by the time-harmonic, quasi-magnetostatic Maxwell equations

$$\nabla \times \left(\mu^{-1}(\boldsymbol{x})\nabla \times \boldsymbol{E}(\boldsymbol{x})\right) - \imath\omega\sigma(\boldsymbol{x})\boldsymbol{E}(\boldsymbol{x}) = \imath\omega\boldsymbol{j}_s(\boldsymbol{x}), \quad \boldsymbol{x} \in D, \tag{2.8}$$

subject to electric boundary conditions

$$\boldsymbol{E}(\boldsymbol{x}) \times \boldsymbol{n}(\boldsymbol{x}) = 0, \quad \boldsymbol{x} \in \partial D, \tag{2.9}$$

where $\boldsymbol{E}$ is the electric field, μ is the magnetic permeability, ω the angular frequency, σ the scalar conductivity field, $\imath$ the imaginary unit and $\boldsymbol{j}_s$ the external current source in the domain D. All physical quantities here and in the rest of this paper are expressed in SI units unless otherwise noted. Note that in this model, displacement currents are neglected, an assumption that is valid in conductors when the conditions $(\omega\tau_E)(\omega\tau_M) \ll 1$ and $\omega\tau_E \ll 1$ are satisfied, where $\tau_E = \epsilon/\sigma$ and $\tau_M = \mu\sigma L^2$ are the electric and magnetic time constants respectively, with ϵ the electric permittivity and L the typical length scale in D.

We will consider a current source that is modelled as a point dipole at source position $\boldsymbol{x}_s$, defined by

$$\boldsymbol{j}_s(\boldsymbol{v}) = (\boldsymbol{p}_s, \delta_{x_s}(\boldsymbol{v})) = (\boldsymbol{p}_s, \boldsymbol{v}(\boldsymbol{x}_s)), \quad \forall \boldsymbol{v} \in C_0^\infty(D, \mathbb{C}^3), \tag{2.10}$$

where $\boldsymbol{p}_s = \|\boldsymbol{p}_s\|_2 \boldsymbol{e}_s$ is the dipole moment along the $\boldsymbol{e}_s$ unit direction, and δ_{x_s} is the Dirac delta distribution centred at the source position. This source model can be considered to validly represent line antennas with length l, for distances $\|\boldsymbol{x}\|_2 \gg l$. In a symmetrical manner, we model measurements of the electric field by a point dipole sensor, at position $\boldsymbol{x}_r \neq \boldsymbol{x}_s$, with $\boldsymbol{p}_r = \boldsymbol{e}_r$, as

$$E_r(\boldsymbol{x}_r) = \overline{\boldsymbol{j}_r(\boldsymbol{E})} = (\delta_{x_r}(\boldsymbol{E}), \boldsymbol{e}_r), \quad \boldsymbol{E} \in C_0^\infty(D, \mathbb{C}^3). \tag{2.11}$$

2.2.1. Weak formulation. We now examine the weak formulation of the problem (see the monographs [54, 50] for a thorough analysis). We assume that $\sigma \in L^\infty(D, \mathbb{R})$ and $\mu^{-1} \in W^{1,\infty}(D, \mathbb{R})$ with

$$0 < \sigma_{\min} = \operatorname*{ess\,inf}_{\boldsymbol{x} \in D} \sigma(\boldsymbol{x}) \leq \operatorname*{ess\,sup}_{\boldsymbol{x} \in D} \sigma(\boldsymbol{x}) = \sigma_{\max} < \infty, \tag{2.12}$$

and

$$0 < \mu_{\min} = \operatorname*{ess\,inf}_{\boldsymbol{x} \in D} \mu(\boldsymbol{x}) \leq \operatorname*{ess\,sup}_{\boldsymbol{x} \in D} \mu(\boldsymbol{x}) = \mu_{\max} < \infty. \tag{2.13}$$

For the space $V = H_0(\operatorname{curl}, D)$, we introduce the sesquilinear form $a : V \times V \to \mathbb{C}$

$$a(\boldsymbol{u}, \boldsymbol{v}; \sigma) = s(\boldsymbol{u}, \boldsymbol{v}) - \imath\omega m(\boldsymbol{u}, \boldsymbol{v}; \sigma), \tag{2.14}$$

where

$$s(\boldsymbol{u},\boldsymbol{v}) = (\mu^{-1}\nabla\times\boldsymbol{u},\nabla\times\boldsymbol{v})_{L^2(D,\mathbb{C}^3)}, \quad m(\boldsymbol{u},\boldsymbol{v};\sigma) = (\sigma\boldsymbol{u},\boldsymbol{v})_{L^2(D,\mathbb{C}^3)}. \tag{2.15}$$

Then the weak formulation becomes: find $\boldsymbol{E}\in V$ such that

$$a(\boldsymbol{E}(\boldsymbol{x}),\boldsymbol{v}(\boldsymbol{x});\sigma(\boldsymbol{x})) = f(\boldsymbol{v}(\boldsymbol{x})), \quad \forall\,\boldsymbol{v}\in V, \tag{2.16}$$

where $f = \imath\omega\boldsymbol{j}_s : V\to\mathbb{C}$ is an antilinear functional, i.e. an element of V^*, the antidual of V. Since the sesquilinear form is continuous and coercive (see Appendix A), the requirements of the Lax-Milgram lemma (see e.g. [60]) are satisfied and therefore the weak problem has a unique solution that obeys the bound

$$\|\boldsymbol{E}\|_V \le \frac{1}{\alpha}\|f\|_{V^*}, \tag{2.17}$$

where α is the coercivity constant and

$$\|f\|_{V^*} = \sup_{\boldsymbol{v}\in V\setminus\{0\}} \frac{|f(\boldsymbol{v})|}{\|\boldsymbol{v}\|_V}, \tag{2.18}$$

is the dual norm. Having acquired a solution to (2.16), we can also define an output functional $s = s(\boldsymbol{E})\in V'$, with V' the dual space of linear bounded functionals on V.

2.2.2. Point source term regularization. For our choice of point dipole source, we have that $\boldsymbol{j}_s\notin V^*$ in three dimensions. To overcome this issue, we employ a regularization of the Dirac delta distribution using the methodology that was suggested in [47]. Since we have the Gelfand triple $C_0^\infty(D,\mathbb{C}^3)\subset V\subset C_0^\infty(D,\mathbb{C}^3)^*$ and $V^*\subset C_0^\infty(D,\mathbb{C}^3)^*$, we construct regularizations $\tilde{\boldsymbol{j}}_H\in V^*$ of $\boldsymbol{j}_s$, with $\tilde{\boldsymbol{j}}_H\to\boldsymbol{j}_s$ as the parameter $H\to 0$ in the weak-$*$ topology (i.e. in distribution) and we take $f = i\omega\tilde{\boldsymbol{j}}_H$. In particular, we define the regularization as

$$\tilde{\boldsymbol{j}}_H(\boldsymbol{v}) = (\boldsymbol{j}_H,\boldsymbol{v})_{L^2(D,\mathbb{C}^3)}, \quad \forall\,\boldsymbol{v}\in V, \tag{2.19}$$

where $\boldsymbol{j}_H = (j_H^1, j_H^2, j_H^3)\in V$ is a compactly supported function within a ball of radius H with centre at $\boldsymbol{x}_s$. Then, since $\tilde{\boldsymbol{j}}_H\in C_0^\infty(D,\mathbb{C}^3)^*$, convergence in the weak-$*$ topology means

$$\tilde{\boldsymbol{j}}_H(\boldsymbol{v})\to\boldsymbol{j}_s(\boldsymbol{v}) = (\boldsymbol{e}_s,\boldsymbol{v}(\boldsymbol{x}_s))_{\mathbb{C}^3}, \quad \forall\,\boldsymbol{v}\in C_0^\infty(D,\mathbb{C}^3) \quad \text{as} \quad H\to 0, \tag{2.20}$$

where we assumed $\|\boldsymbol{p}_s\|_2 = 1$. Using the m-th order Taylor expansion for $\boldsymbol{v}(\boldsymbol{x})$ around the point $\boldsymbol{x}_s$ to substitute in (2.19) and comparing with (2.20), we arrive at the compact m-moment conditions

$$(j_H^i,\chi_D)_{L^2(D)} = e_s^i \quad \text{and} \quad (j_H^i,(\boldsymbol{x}-\boldsymbol{x_s})^{\boldsymbol{\alpha}})_{L^2(D)} = 0, \quad i=1,2,3, \quad 1\le|\boldsymbol{\alpha}|\le m, \tag{2.21}$$

where χ_D is the indicator function in D. The convergence $|\boldsymbol{j}_s(\boldsymbol{v})-\tilde{\boldsymbol{j}}_H(\boldsymbol{v})|$ can then be estimated to be of order $O(H^{m+1})$. In practice, we use an expansion of j_H in terms of an appropriate basis and then solve the linear system that is derived from the moment conditions. In the numerical examples, we make use of a spherically symmetric approximation based on shifted Legendre polynomials.

Remark 2.1. The study of convergence in weighted Sobolev norms is beyond the scope of this paper; we expect that results similar to the case in [47] hold, i.e. the same moment conditions as (2.21) need to be satisfied and the convergence rate suggests that the support H is chosen to be comparable to the (local) mesh size h around the source position.

2.2.3. Pointwise measurement regularization. Pointwise values of solutions to (2.16) are rigorously justified only when the solution is sufficiently regular (see [2] for conditions), so our measurement model is problematic in general when applied to the weak formulation. In other words, our requirement that the output functional s is bounded is not true for point measurements as in (2.11). Therefore, we employ the same regularization technique as for the source term to obtain a regularized linear functional $\tilde{\boldsymbol{s}}_H \in V'$ with $\tilde{\boldsymbol{s}}_H \to \boldsymbol{j}_r$ as $H \to 0$, defined in this case by

$$\tilde{\boldsymbol{s}}_H(\boldsymbol{v}) = (\boldsymbol{v}, \boldsymbol{s}_H)_{L^2(D,\mathbb{C}^3)}, \quad \forall \boldsymbol{v} \in V, \tag{2.22}$$

where $\boldsymbol{s}_H \in V$ is a compactly supported function within a ball of radius H around $\boldsymbol{x}_r$. This leads to compact moment conditions, similar to (2.21). We then set $s = \tilde{\boldsymbol{s}}_H$ when we want to consider pointwise measurements.

2.3. Stochastic model. We assume that there are two subdomains D_+ and D_- of D, such that $D_+ \cap D_- = \emptyset$, $\overline{D}_+ \cup \overline{D}_- = \overline{D}$ with polyhedral interface $\Gamma = \overline{D}_+ \cap \overline{D}_-$. In D_+ which represents e.g. a sea layer in CSEM, we assume we have knowledge of a constant conductivity value $\sigma_+ > 0$, while in D_- (e.g. the subsurface) the lack of knowledge leads us to model the conductivity as a spatial random field $\sigma_-(\boldsymbol{x}, \theta)$ in a probability space $(\Theta, \Sigma, \mathbb{P})$. Furthermore, to enforce positivity we assume $\sigma_-(\boldsymbol{x}, \theta)$ is lognormal, so that we write

$$\sigma(\boldsymbol{x}, \theta) = \begin{cases} \sigma_+ & \boldsymbol{x} \in D_+, \\ \sigma_-(\boldsymbol{x}, \theta) & \boldsymbol{x} \in D_-, \theta \in \Theta, \end{cases} \tag{2.23}$$

with

$$\sigma_-(\boldsymbol{x}, \theta) = \sigma_*(\boldsymbol{x}) + \sigma_0(\boldsymbol{x}) \exp(q(\boldsymbol{x}, \theta)), \tag{2.24}$$

where $\sigma_*(\boldsymbol{x})$ and $\sigma_0(\boldsymbol{x})$ are continuous functions in $\overline{D}_-$ that are non-negative and strictly positive respectively. The random field $q(\boldsymbol{x}, \theta) \in L^2(\Theta, L^2(D_-))$ is a Gaussian, mean-zero field with stationary covariance function $C_q(\boldsymbol{x}, \boldsymbol{y})$ that belongs to the Whittle-Matérn class

$$C_q(\boldsymbol{x}, \boldsymbol{y}) = \frac{\mathrm{Var}[q]}{2^{\nu-1}\Gamma(\nu)} \left(\|\boldsymbol{x} - \boldsymbol{y}\|_M\right)^{\nu} K_\nu \left(\|\boldsymbol{x} - \boldsymbol{y}\|_M\right), \quad \boldsymbol{x}, \boldsymbol{y} \in D_- \tag{2.25}$$

where $\nu > 0$ is a smoothness parameter, K_ν is the modified Bessel function of the second kind of order ν and $\|\boldsymbol{x}\|_M^2 = \boldsymbol{x}^T M^{-1} \boldsymbol{x}$ is the weighted Euclidean norm with $M \in \mathbb{R}^{3\times 3}$ a constant, symmetric, positive definite matrix. Note that this covariance function is in general anisotropic; the usual isotropic case with length scale l occurs when $M = l^2 I_3$ or by use of scaling as $M = (l/2\nu)^2 I_3$. For the isotropic case, it is well known that the random field $q(\boldsymbol{x}, \theta)$ is $n < \nu$ mean-square differentiable and we also have that (see [51, 15]) a.e. in Θ

$$\mathbb{E}[|q(\boldsymbol{x}) - q(\boldsymbol{y})|^2] \leq L \|\boldsymbol{x} - \boldsymbol{y}\|_2^s, \quad \forall \boldsymbol{x}, \boldsymbol{y} \in \overline{D}_-, \tag{2.26}$$

for some $L > 0$ and all s such that $s \leq 2\nu$ and $s \in (0, 2)$. Now, given realizations $\sigma(\cdot, \theta)$, we seek random field realizations $\boldsymbol{E}(\cdot, \theta) \in V$ such that

$$a(\boldsymbol{E}(\boldsymbol{x}, \theta), \boldsymbol{v}(\boldsymbol{x}); \sigma(\boldsymbol{x}, \theta)) = f(\boldsymbol{v}(\boldsymbol{x})), \quad \forall \boldsymbol{v} \in V, \tag{2.27}$$

for almost all $\theta \in \Theta$.

Proposition 2.2. *The random field $\boldsymbol{E}(\boldsymbol{x},\theta)$ defined as a measurable mapping $\boldsymbol{E}: D\times\Theta\to V$ such that for almost all $\theta\in\Theta$, it is the solution of (2.27), has finite moments i.e. $\|\boldsymbol{E}\|_{L^p(\Theta,V)}<\infty$ for all $0\le p\le\infty$.*

Proof. We follow [16, Proposition 2.1]. For the stationary covariance $C_q(\boldsymbol{x},\boldsymbol{y})=c(\|\boldsymbol{x}-\boldsymbol{y}\|_M)$ in (2.25), we have

$$\begin{aligned}\mathbb{E}[|q(\boldsymbol{x})-q(\boldsymbol{y})|^2] &= 2(c(\boldsymbol{0})-c(\|\boldsymbol{x}-\boldsymbol{y}\|_M))\\ &= 2(c(0)-c(\|\boldsymbol{x}'-\boldsymbol{y}'\|_2))\\ &\le K\|\boldsymbol{x}'-\boldsymbol{y}'\|_2^s = K\|\boldsymbol{x}-\boldsymbol{y}\|_M^s\\ &\le K\|\boldsymbol{x}-\boldsymbol{y}\|_2^s,\quad s\le 2\nu, s\in(0,2),\ \forall \boldsymbol{x},\boldsymbol{y}\in\overline{D}_-\end{aligned}\tag{2.28}$$

where we used property (2.26) of the isotropic covariance and the equivalence of the norms. Therefore, the Kolmogorov continuity theorem (see [56, Theorem 3.5]) applies and there is a version of q with realizations which are almost surely Hölder continuous with an exponent $\beta\le\min(\nu,1)$ (i.e. in $C^{0,\beta}(\overline{D}_-)$). Under the continuity assumptions on σ_0 and σ_*, $\sigma_-(\boldsymbol{x},\theta)$ is also Hölder-continuous with exponent β and we also have that a.e. in Θ

$$0<\sigma_{\min}(\theta)=\operatorname*{ess\,inf}_{\boldsymbol{x}\in D}\sigma(\boldsymbol{x},\theta)\le\sigma(\boldsymbol{x},\theta)\le\operatorname*{ess\,sup}_{\boldsymbol{x}\in D}\sigma(\boldsymbol{x},\theta)=\sigma_{\max}(\theta)<\infty,\quad \text{a.e. in } D.\tag{2.29}$$

Fixing any θ and applying the Lax-Milgram lemma as in the deterministic case, we have the $\mathbb{P}$-a.s. uniqueness of the solution $\boldsymbol{E}(\cdot,\theta)$ with the bound

$$\|\boldsymbol{E}(\cdot,\theta)\|_V\le\frac{1}{\alpha(\theta)}\|f\|_{V^*},\tag{2.30}$$

where we take $\alpha(\theta)=(\mu_{\max}^2+(\omega\sigma_{\min}(\theta))^{-2})^{-1/2}$. From Fernique's theorem (see e.g. [67]), it can be derived as in [16, Proposition 2.3] that the random variables $\sigma_{\min}^\lambda(\theta)$ and $\sigma_{\max}^\lambda(\theta)$ are in $L^p(\Theta)$ for any $p\ge0$ and $\lambda\in\mathbb{R}$. Therefore we have that

$$\mathbb{E}\left[\|\boldsymbol{E}\|_V^p\right]\le\mathbb{E}\left[\alpha(\theta)^{-p}\right]\|f\|_{V^*}^p,\tag{2.31}$$

and since $\alpha(\theta)^{-1}\in L^p(\Theta)$ we get the finiteness of all moments

$$\|\boldsymbol{E}\|_{L^p(\Theta,V)}\le\|\alpha(\theta)^{-1}\|_{L^p(\Theta)}\|f\|_{V^*},\quad 0\le p<\infty.\tag{2.32}$$

■

Remark 2.3. The preceding as well as the following methodology and analysis are also valid if one considers a random field that occupies the whole domain D. The case of random fields defined in different layers with known discontinuity interfaces is also interesting and could be treated using the approach presented in this paper with the necessary assumptions and modifications.

2.4. Deterministic, parametric representation. To achieve a parametric representation, we use the Karhunen-Loève expansion to write

$$q(\boldsymbol{x},\theta)=\sum_{j=1}^{\infty}\sqrt{\lambda_j}\phi_j(\boldsymbol{x})\xi_j(\theta),\quad \boldsymbol{x}\in D_-,\theta\in\Theta,\tag{2.33}$$

where the sum converges in $L^2(\Theta; L^2(D_-))$, $\lambda_j \in l^1(\mathbb{N})$ are the eigenvalues with $\lambda_1 \geq \lambda_2 \geq \cdots \geq 0$ and ϕ_j are the $L^2(D_-)$-orthonormal eigenfunctions of the covariance operator $\mathcal{C}_q$ with kernel C_q. The random variables $y_j = \xi_j(\theta)$ are i.i.d and distributed as $N(0,1)$. By defining $\psi_j = \sqrt{\lambda_j}\phi_j$, we get the parametric expression

$$\sigma_-(\boldsymbol{x}, \boldsymbol{y}) = \sigma_*(\boldsymbol{x}) + \sigma_0(\boldsymbol{x}) \exp\left(\sum_{j=1}^{\infty} y_j \psi_j(\boldsymbol{x})\right), \quad \boldsymbol{x} \in D_-, \tag{2.34}$$

with the random vector $\boldsymbol{y}$ defined on the measure space $(U, \mathcal{B}(U), \gamma_G)$, where $U = \mathbb{R}^{\mathbb{N}}$, $\mathcal{B}(U)$ is the σ-algebra generated by the Borel cylinders and $\gamma_G = \otimes_{j=1}^{\infty} \mathrm{N}(0,1)$ is the countable tensor product Gaussian measure. We can write

$$\sigma(\boldsymbol{x}, \boldsymbol{y}) = \sigma_+ \chi_{D_+}(\boldsymbol{x}) + \sigma_-(\boldsymbol{x}, \boldsymbol{y}) \chi_{D_-}(\boldsymbol{x}), \quad \boldsymbol{x} \in D,\ \boldsymbol{y} \in U. \tag{2.35}$$

Truncated expressions can be understood by setting $\boldsymbol{y} = \boldsymbol{y}_J = (y_1, \ldots, y_J, 0, \ldots)$. The variational problem now becomes: given $\boldsymbol{y} \in U$, find $\boldsymbol{E}(\cdot, \boldsymbol{y}) \in V$ such that

$$a(\boldsymbol{E}(\boldsymbol{x}, \boldsymbol{y}), \boldsymbol{v}(\boldsymbol{x}); \sigma(\boldsymbol{x}, \boldsymbol{y})) = f(\boldsymbol{v}(\boldsymbol{x})), \quad \forall \boldsymbol{v} \in V. \tag{2.36}$$

The measurability of the maps $\boldsymbol{y} \to \sigma(\cdot, \boldsymbol{y})$ and $\boldsymbol{y} \to \boldsymbol{E}(\cdot, \boldsymbol{y})$ and the finiteness of $\|\boldsymbol{E}\|_{L^p(U,V)}$ requires that

$$q(\boldsymbol{x}, \boldsymbol{y}) = \sum_{j=1}^{\infty} y_j \psi_j(\boldsymbol{x}) \in L^\infty(D_-), \quad \text{and} \quad \mathbb{E}(\exp(p\|q(\boldsymbol{x}, \boldsymbol{y})\|_{L^\infty(D_-)})) < \infty, \quad 0 \leq p < \infty, \tag{2.37}$$

which can be derived from Hölder continuity as in the stochastic case (see e.g. [40]). Then uniqueness of weak solutions to problem (2.36) is guaranteed from the Lax-Milgram lemma and

$$\|\boldsymbol{E}\|_{L^p(U,V)} \leq \|\alpha(\boldsymbol{y})^{-1}\|_{L^p(U)} \|f\|_{V^*}, \quad \forall \boldsymbol{y} \in U,\ 0 \leq p < \infty, \tag{2.38}$$

where we take $\alpha(\boldsymbol{y}) = (\mu_{\max}^2 + (\omega \sigma_{\min}(\boldsymbol{y}))^{-2})^{-1/2}$ with

$$\sigma_{\min}(\boldsymbol{y}) = \min(\sigma_+, \operatorname*{ess\,inf}_{\boldsymbol{x} \in D_-} \sigma_-(\boldsymbol{x}, \boldsymbol{y})), \tag{2.39}$$

and

$$\operatorname*{ess\,inf}_{\boldsymbol{x} \in D_-} \sigma_-(\boldsymbol{x}, \boldsymbol{y}) \geq \operatorname*{ess\,inf}_{\boldsymbol{x} \in D_-} \sigma_*(\boldsymbol{x}) + \operatorname*{ess\,inf}_{\boldsymbol{x} \in D_-} \sigma_0(\boldsymbol{x}) \exp\left(-\|q(\boldsymbol{x}, \boldsymbol{y})\|_{L^\infty(D_-)}\right). \tag{2.40}$$

Note also that the continuity factor is $\gamma(\boldsymbol{y}) = \max(\mu_{\min}^{-1}, \omega \sigma_{\max})$ with

$$\sigma_{\max} = \max(\sigma_+, \operatorname*{ess\,sup}_{\boldsymbol{x} \in D_-} \sigma_-(\boldsymbol{x}, \boldsymbol{y})), \tag{2.41}$$

and

$$\operatorname*{ess\,sup}_{\boldsymbol{x} \in D_-} \sigma_-(\boldsymbol{x}, \boldsymbol{y}) \leq \operatorname*{ess\,sup}_{\boldsymbol{x} \in D_-} \sigma_*(\boldsymbol{x}) + \operatorname*{ess\,sup}_{\boldsymbol{x} \in D_-} \sigma_0(\boldsymbol{x}) \exp\left(\|q(\boldsymbol{x}, \boldsymbol{y})\|_{L^\infty(D_-)}\right). \tag{2.42}$$

An alternative sufficient condition is given in [6]:

Assumption 2.4. *Assume there is a positive sequence* $(\rho_j)_{j\geq 1}$ *such that*

$$\sum_{j=1}^{\infty} \rho_j |\psi_j(\boldsymbol{x})| \in L^\infty(D_-) \quad \textit{and} \quad \sum_{j=1}^{\infty} \exp(-\rho_j^2) < \infty. \tag{2.43}$$

Then uniqueness is guaranteed and (2.38) is again true. For our specific choice of C_q, the norms $\|\psi_j\|_{L^\infty(D_-)}$ are bound as (see Appendix B)

$$\|\psi_j(\boldsymbol{x})\|_{L^\infty(D_-)} \leq K j^{-\nu/3+\epsilon}, \quad \epsilon > 0,\ K > 0. \tag{2.44}$$

This indicates that Assumption 2.4 is satisfied for $\nu > 3$. In the following, we will assume this level of smoothness which does not allow for rough random fields with e.g. exponential covariance function. Note that the same properties are also shared by the truncated solution $\boldsymbol{E}_J$ when using a truncated representation $\sigma_J = \sigma(\cdot, \boldsymbol{y}_J)$.

2.4.1. Quantities of Interest. Having described the deterministic, parametric problem with distributed uncertainty, the quantification of the propagated uncertainty in the output functional s is obtained from the calculation of some Quantity of Interest (QoI), which is an infinite-dimensional integration problem with respect to the prior measure. We will focus on the second order characterization of s, which requires the calculation of the following QoIs

$$\mathbb{E}[s] = \int_U s(\boldsymbol{E}(\boldsymbol{y}))\, d\gamma_G(\boldsymbol{y}), \tag{2.45}$$

$$\mathrm{Cov}[s, \overline{s}] = \mathbb{E}[(s - \mathbb{E}[s])\overline{(s - \mathbb{E}[s])}], \tag{2.46}$$

$$\mathrm{Cov}[s, s] = \mathbb{E}[(s - \mathbb{E}[s])(s - \mathbb{E}[s])], \tag{2.47}$$

i.e. the mean, covariance and pseudo-covariance of s respectively. For any integral of this type we denote the integrand as $z(\boldsymbol{E}(\boldsymbol{y}))$ (e.g. $z = s$ for the mean of s). In practice, (2.45) becomes a high-dimensional integration problem which needs a correspondingly high number of computationally expensive deterministic solutions of (2.36). Next, we describe the method that we will use to numerically approximate the integrals.

3. Approximation methodology.

In this section we describe the approximation methods for the estimation of the QoIs, namely the Sparse Quadrature (SQ) and model reduction methods.

3.1. Sparse Quadrature.

Sparse Quadrature, in its generalized form, is defined in terms of a sum of operators on downward closed index sets $\Lambda \subset \mathcal{F}$ which obey the condition

$$\text{if} \quad \boldsymbol{\nu} \in \Lambda \quad \text{and} \quad \boldsymbol{\mu} \leq \boldsymbol{\nu}, \quad \text{then} \quad \boldsymbol{\mu} \in \Lambda. \tag{3.1}$$

Following [17], we begin by defining for a level $l \geq 0$, a sequence of m_l univariate quadrature points $(y_k^l)_{k=0}^{m_l-1} \in \mathbb{R}$ and weights $(w_k^l)_{k=0}^{m_l-1} \in \mathbb{R}$ with $m_0 = 1, y_0^0 = 0, w_0^0 = 1$ and $m_l < m_{l+1}$. Then we approximate $\mathbb{E}[f]$ for a Banach space valued function $f \in L^2(\mathbb{R}, S, g(y)dy) = L^2(\mathbb{R}, g(y)dy) \otimes S$, with $g(y) = (2\pi)^{-1/2} \exp(-y^2/2)$ being the standard univariate Gaussian density, by the quadrature operator at level l

$$\mathcal{Q}_l[f] = \sum_{k=0}^{m_l-1} w_k^l f(y_k^l), \tag{3.2}$$

with the convention that $\mathcal{Q}_{-1}[f] = 0$.

Remark 3.1. The points and weights are obtained by a quadrature rule that is suitable for integrals with Gaussian measure such the Gauss-Hermite, Genz-Keister, weighted Leja and transformed Gauss-Kronrod-Patterson quadrature rules. The specific choice affects the quality of the approximation (stability, convergence) and the computational cost (nested or non-nested, growth of m_l).

We also make the following assumption regarding the quadrature approximation.

Assumption 3.2. *(cf. [17, Assumption 1])*

$$\mathbb{E}[f] = \mathcal{Q}_l(f), \quad \forall f \in \mathbb{P}_l \otimes S, \tag{3.3}$$

where $\mathbb{P}_l = \text{span}\{y^i, 0 \leq i \leq l\}$ *and*

$$|\mathcal{Q}_l(H_n)| \leq 1, \quad \forall l \geq 0 \quad \textit{and} \quad \forall n \geq l, \tag{3.4}$$

where H_n *are the Hermite polynomials, orthonormal in* $L^2(\mathbb{R}, g(y)dy)$*, defined as*

$$H_n(y) = \frac{(-1)^n g^{(n)}(y)}{\sqrt{n!}g(y)}. \tag{3.5}$$

The condition in (3.3) is satisfied by Gauss-Hermite and Genz-Keister rules for $m_l = l+1$ but is not satisfied in general by the weighted Leja rule. As is known, Gauss-Hermite quadrature with m points is exact for polynomials of degree up to $2m-1$. The bound in (3.4) (see also [35] for a more general condition) has been verified numerically for Gauss-Hermite and Genz-Keister quadrature for all possible l and n up to machine precision (see [17]). We have also verified it for the weighted Leja rule up to $l = 70$ and $n = 200$ with precision equal to 256 digits. Alternatively a relaxed version of (3.4), given by $|\mathcal{Q}_l(H_n)| \leq 2$, has been proven in [17] for the Gauss-Hermite rule. In the multivariate case, for $\boldsymbol{\nu} \in \mathcal{F}$ we define a Cartesian product grid

$$G_{\boldsymbol{\nu}} = \prod_{j \geq 1} (y_{k_j}^{\nu_j})_{k_j=0}^{m_{\nu_j}-1} \subset U, \tag{3.6}$$

and the sparse grid as

$$G_\Lambda = \bigcup_{\boldsymbol{\nu} \in \Lambda} G_{\boldsymbol{\nu}}. \tag{3.7}$$

The associated SQ approximation to $\mathbb{E}[f]$ for some function $f \in L^2(U, S, \gamma_G)$ is given by

$$\mathcal{Q}_\Lambda[f] = \sum_{\boldsymbol{\nu} \in \Lambda} \Delta_{\boldsymbol{\nu}}[f], \tag{3.8}$$

where $\Delta_{\boldsymbol{\nu}}$ are the tensorised, multivariate quadrature difference operators defined as

$$\Delta_{\boldsymbol{\nu}}[f] = \bigotimes_{j \geq 1} \Delta_{\nu_j}[f] = \bigotimes_{j \geq 1} (\mathcal{Q}_{\nu_j} - \mathcal{Q}_{\nu_j - 1})[f] = \sum_{\boldsymbol{\nu} - \boldsymbol{\mu} = \mathbf{1}}^{\boldsymbol{\nu} - \boldsymbol{\mu} = \mathbf{1}} (-1)^{|\boldsymbol{\nu} - \boldsymbol{\mu}|} \mathcal{Q}_{\boldsymbol{\mu}}[f], \tag{3.9}$$

and where the tensorised, multivariate quadrature operators are

$$\mathcal{Q}_{\boldsymbol{\nu}}[f] = \bigotimes_{j\geq 1} \mathcal{Q}_{\nu_j}[f] = \sum_{k_{j_1}=0}^{m_{\nu_{j_1}}-1} \cdots \sum_{k_{j_n}=0}^{m_{\nu_{j_n}}-1} w_{k_{j_1}}^{\nu_{j_1}} \dots w_{k_{j_n}}^{\nu_{j_n}} f(y_{k_{j_1}}^{\nu_{j_1}}, \dots, y_{k_{j_n}}^{\nu_{j_n}}), \tag{3.10}$$

where in the last term we used the convention that $\operatorname{supp}(\boldsymbol{\nu}) = (j_1, \dots, j_n)$ and that we set $y_j = 0$ for $j \notin \operatorname{supp}(\boldsymbol{\nu})$.

3.1.1. Convergence of SQ. Since $f \in L^2(U, S, \gamma_G)$, we can use Hermite polynomials $H_{\boldsymbol{\nu}}$, that constitute a basis for $L^2(U, \gamma_G)$, to write

$$f(\boldsymbol{y}) = \sum_{\boldsymbol{\nu}\in\mathcal{F}} f_{\boldsymbol{\nu}} H_{\boldsymbol{\nu}}(\boldsymbol{y}), \quad f_{\boldsymbol{\nu}} = \int_U f(\boldsymbol{y}) H_{\nu}(\boldsymbol{y})\, d\gamma_G(\boldsymbol{y}), \quad H_{\boldsymbol{\nu}}(\boldsymbol{y}) = \prod_{j\geq 1} H_{\nu_j}(y_j). \tag{3.11}$$

The best N-term approximation is obtained by replacing $\mathcal{F}$ with an index set Λ_N with $\#(\Lambda_n) = N$, which corresponds to the N largest norms $\|f_{\boldsymbol{\nu}}\|_S$. The work in [6] (see also [29]) proves that under certain assumptions, best N-term Hermite approximations converge in $L^2(U, S, \gamma_G)$ with dimension independent rates. In our case, we are interested in the closely related convergence of the SQ approximation. This is analysed in [17], where a dimension independent rate is proved (a similar analysis for generalized sparse grid interpolation appears in [35]). In particular, the theorem relies on Assumption 3.2 and on the additional assumption

Assumption 3.3. *(cf. [17, Assumption 2]) Let $0 < p < 1$, $q = q(p) = 2p/(2-p)$ and r the smallest integer such that $r > 10/q$. Assume that there exists a positive sequence $(\rho_j)_{j\geq 1}$ such that $(\rho_j^{-1})_{j\geq 1} \in l^q(\mathbb{N})$ and additionally*

$$\sum_{\|\boldsymbol{\mu}\|_{l^\infty}\leq r} \frac{\boldsymbol{\rho}^{2\boldsymbol{\mu}}}{\boldsymbol{\mu}!} \int_U \|\partial^{\boldsymbol{\mu}} f(\boldsymbol{y})\|_S^2\, d\gamma_G(\boldsymbol{y}) < \infty. \tag{3.12}$$

Note that here $r > 10/q$ instead of $r > 14/q$ in [17] due to allowing the sharper (numerically verified) bound in (3.4).

Theorem 3.4. *([17, Theorem 3.6]) Under Assumption 3.2 and Assumption 3.3, for any $N \in \mathbb{N}$, there exists a downward closed index set $\Lambda_N \in \mathcal{F}$, corresponding to the set of indices with the N smallest values of $b_{\boldsymbol{\mu}}$ defined as*

$$b_{\boldsymbol{\mu}} = \sum_{\|\tilde{\boldsymbol{\mu}}\|\leq r} \binom{\boldsymbol{\mu}}{\tilde{\boldsymbol{\mu}}} \boldsymbol{\rho}^{2\tilde{\boldsymbol{\mu}}}, \tag{3.13}$$

such that

$$\|\mathbb{E}[f] - \mathcal{Q}_{\Lambda_N}[f]\|_S \leq K(N+1)^{-s}, \quad s = \frac{1}{p} - 1, \tag{3.14}$$

where K is independent of N.

To prove Theorem 3.4 applies for the model we are examining in this paper with $f = \boldsymbol{E}$ and $S = V$ or $f = s(\boldsymbol{E}), s \in V'$ and $S = \mathbb{C}$, we will employ a slightly modified version of an assumption given in [6]:

Assumption 3.5. *(cf. [6, Theorem 1.2]) Let $0 < p < 1$, $q = q(p) = 2p/(2-p)$. Assume that there exists a positive sequence $(\rho_j)_{j\geq 1}$ such that $(\rho_j^{-1})_{j\geq 1} \in l^q(\mathbb{N})$ and additionally*

$$\sup_{\boldsymbol{x}\in D_-} \sum_{j=1}^{\infty} \rho_j |\psi_j(\boldsymbol{x})| < \infty. \tag{3.15}$$

If the above Assumption 3.5 holds, then as discussed in [6] for $0 < p < 2$, the validity of Assumption 2.4 follows and therefore the well-posedness of the parametric problem and the finiteness of all moments of the solution are guaranteed.

Theorem 3.6. *If Assumption 3.5 is satisfied for the parametric representation of the conductivity given by (2.34), then Assumption 3.3 is also satisfied with $f = \boldsymbol{E}$ and $S = V$. Therefore, assuming also the validity of Assumption 3.2, Theorem 3.4 applies for the estimation of the prior mean of the solution $\boldsymbol{E}$ of (2.36) as in (2.45).*

Proof. See Appendix C. ∎

For our choice of parametric representation through the Karhunen-Loève expansion, we can see that if $\nu > 3/r$ for some $0 < r < 2/3$, then $(\|\psi_j\|_{L^\infty})_{j\geq 1} \in l^r(\mathbb{N})$, and we can choose $\rho_j = \|\psi_j\|_{L^\infty}^{r-1}$ so that Assumption 3.5 is satisfied and $(\rho_j^{-1})_{j\geq 1} \in l^q$, with $q = r/(1-r)$. Then we obtain the convergence rate $s = \frac{1}{r} - \frac{3}{2}$. Therefore, the SQ approximation for the parametric model is guaranteed to have a dimension independent convergence rate that is better than the convergence rate $O(N^{-1/2})$ of the Monte Carlo method when $0 < r < 1/2$ or $\nu > 6$. In practice the convergence may be faster since some of the bounds in the analysis may not be sharp.

The construction of the index sets Λ can proceed in an a priori or a posteriori method. An adaptive a priori construction is proposed in [17] and is based on the previous analysis and the selection of the coefficients b_μ in (3.13) with the smallest value among a possible candidate set. In this paper we focus instead on an a posteriori construction that is based on the dimension-adaptive algorithm originally found in [36] (see also [24, 62]). This heuristic algorithm identifies important dimensions in U using a suitable a posteriori error indicator and proceeds to enrich the index set accordingly.

In the case of a Gauss-Hermite, non-nested quadrature rule with $m_{l+1} = m_l + 1$, we mention the results in [35], which give the bound $|G_{\Lambda_N}| \leq N(N+1)/2$ for the number of sparse grid points. This allows to express the convergence rate (3.14) in terms of the number points (or equivalently the number of function evaluations) as

$$\|\mathbb{E}[f] - \mathcal{Q}_{\Lambda_N}[f]\|_S \leq K|G_{\Lambda_N}|^{-\tilde{s}}, \quad \tilde{s} = \frac{1}{2p} - \frac{1}{2}. \tag{3.16}$$

Note that we do not employ an a priori, fixed truncation level for the parametric representation but we start from J dimensions and we extend the truncation to $J = J + 1$ when some dimension $j \leq J$ becomes active (i.e. when $\nu_j = 1$). We make use of the concepts of the (restricted to J dimensions) margin, reduced margin and neighbours of an index set (see e.g. [55]). The margin of an index set Λ is defined as

$$M_\Lambda = \{\boldsymbol{\nu} \notin \Lambda : \exists \boldsymbol{\mu} \in \Lambda : |\boldsymbol{\nu} - \boldsymbol{\mu}| = 1 \quad \text{and} \quad \mu_j = 0, \nu_j = 0, \forall j > J\}. \tag{3.17}$$

The reduced margin is the subset of the margin of Λ defined as

$$R_\Lambda = \{\boldsymbol{\nu} \notin \Lambda : \boldsymbol{\nu} - \boldsymbol{e}_j \in \Lambda, \forall j \in \mathrm{supp}(\boldsymbol{\nu}) \quad \text{and} \quad \nu_j = 0, \forall j > J\}, \tag{3.18}$$

i.e. it contains all the (restricted) indices $\boldsymbol{\nu}$ such that $\Lambda \cup \{\boldsymbol{\nu}\}$ remains downward closed. Finally, the neighbours $N(\boldsymbol{\mu}, \Lambda)$ of $\boldsymbol{\mu}$ with respect to Λ are defined as

$$N(\boldsymbol{\mu}, \Lambda) = \{\boldsymbol{\nu} \notin \Lambda : |\boldsymbol{\nu} - \boldsymbol{\mu}| = 1 \quad \text{and} \quad \mu_j = 0, \nu_j = 0, \forall j > J\}. \tag{3.19}$$

Since in general, we have

$$\|\mathbb{E}[f] - \mathcal{Q}_\Lambda[f]\|_S \leq \sum_{\boldsymbol{\nu} \notin \Lambda} \|\Delta_{\boldsymbol{\nu}}[f]\|_S \,, \tag{3.20}$$

we use $\|\Delta_{\boldsymbol{\nu}}[f]\|_S$ as the error indicator for an index $\boldsymbol{\nu} \in R_\Lambda$. The algorithm first assigns the error contribution to every index in R_Λ, then moves the index with the highest contribution from R_Λ to Λ, updates R_Λ and finally proceeds to the next step. Note that we could also assign a work contribution (e.g. number of additional points added to sparse grid) to each index in R_Λ and then choose the index with the highest profit (error contribution/work contribution). We postpone the presentation of the complete algorithm for subsection 3.3, since we first describe additional approximations in the next section with the aim of further reducing the computational cost for the approximation of the QoIs, following ideas proposed in [18] for UQ and also in [21, 22] for the Bayesian inverse problem.

3.2. Model reduction. We obtain the so-called High Fidelity (Hi-Fi) solutions to (2.36) by the Finite Element Method (FEM) on a tetrahedral mesh $\mathcal{T}_h$ for the domain D. In particular we use a finite element space V_h with $\dim(V_h) = N_h$, that is spanned by the lowest-order Nédélec curl-conforming edge elements $\boldsymbol{N}_i$ (see [54]). The FEM approximation $\boldsymbol{E}_h(\boldsymbol{y}) = \sum_{j=1}^{N_h} e_h^j(\boldsymbol{y})\boldsymbol{N}_j$ is obtained by solving the discrete variational problem: given any $\boldsymbol{y} \in U$, find $\boldsymbol{E}_h(\boldsymbol{y}) \in V_h$ such that

$$\begin{aligned} a(\boldsymbol{E}_h(\boldsymbol{y}), \boldsymbol{v}_h; \sigma(\boldsymbol{y})) &= s(\boldsymbol{E}_h(\boldsymbol{y}), \boldsymbol{v}_h) - \imath\omega m(\boldsymbol{E}_h(\boldsymbol{y}), \boldsymbol{v}_h; \sigma(\boldsymbol{y})) \\ &= s(\boldsymbol{E}_h(\boldsymbol{y}), \boldsymbol{v}_h) - \imath\omega m(\boldsymbol{E}_h(\boldsymbol{y}), \boldsymbol{v}_h; \sigma_+\chi_{D_+}) - \imath\omega m(\boldsymbol{E}_h(\boldsymbol{y}), \boldsymbol{v}_h; \sigma_-(\boldsymbol{y})\chi_{D_-}) \\ &= f(\boldsymbol{v}_h), \quad \forall \boldsymbol{v}_h \in V_h, \end{aligned} \tag{3.21}$$

which translates into the following symmetric, non-hermitian, indefinite and sparse linear system

$$\mathrm{A}_h(\boldsymbol{y})\boldsymbol{e}_h(\boldsymbol{y}) = (\mathrm{S} - \imath\omega\mathrm{M}_+ - \imath\omega\mathrm{M}(\boldsymbol{y}))\boldsymbol{e}_h(\boldsymbol{y}) = \boldsymbol{b}, \tag{3.22}$$

with

$$(\mathrm{S})_{ij} = s(\boldsymbol{N}_j, \boldsymbol{N}_i), \quad i, j = 1, \ldots, N_h, \tag{3.23}$$

$$(\mathrm{M}_+)_{ij} = m(\boldsymbol{N}_j, \boldsymbol{N}_i; \sigma_+\chi_{D_+}), \quad i, j = 1, \ldots, N_h, \tag{3.24}$$

$$(\mathrm{M}(\boldsymbol{y}))_{ij} = m(\boldsymbol{N}_j, \boldsymbol{N}_i; \sigma_-(\boldsymbol{y})\chi_{D_-}), \quad i, j = 1, \ldots, N_h, \tag{3.25}$$

$$(\boldsymbol{b})_i = f(\boldsymbol{N}_i), \quad i = 1, \ldots, N_h. \tag{3.26}$$

The well-posedness of (3.21) is inherited from the abstract weak formulation for sufficiently fine mesh size h and the solution obeys optimal error estimates as proved in [72].

Although as we have seen in the previous section, sparse grid quadrature can achieve dimension independent rates, the computational cost is still high when a large number of linear solves to (3.22) is required. For this reason, we employ a (projection-based) model reduction to obtain a Low-Fidelity (Low-Fi) representation of (3.22) on a subspace $V_{N_P} \subset V_h$ with $\dim(V_{N_P}) = N_P \ll N_h$. Thus, we replace the Hi-Fi model in the calculation of the QoI with a Low-Fi model, with *controlled levels of accuracy and computational cost*. As we describe in the next sections, the resulting reduced model is affine and allows the calculation of all $\boldsymbol{y}$-independent, N_h-dimensional quantities during an offline phase and the fast online evaluation of the solution for any $\boldsymbol{y}$ using only N_P-dimensional expressions.

As a preliminary step, we define the parametrized set $\mathcal{X} = \{\sigma_-(\cdot, \boldsymbol{y}) : \boldsymbol{y} \in U\} \subset C(\overline{D}_-) \subset L^\infty(D_-)$ and the solution manifold $\mathcal{M} = \{\boldsymbol{E}(\cdot, \boldsymbol{y}) : \boldsymbol{y} \in U\} \subset H(\mathrm{curl}; D)$. We will use model reduction schemes with the goal of finding approximations to these sets. Since the underlying parameter space U is not compact, we will seek approximations as measured in a weighted norm. The rationale behind this approach is based on i) the fast decay of the Kolmogorov n-width, or more appropriate in our case, the p-average n-widths[1] of the particular sets and the regularity and anisotropy of the maps with respect to $\boldsymbol{y}$ (see e.g. [57, 33]) and on ii) (weak) greedy algorithms that have been shown in [13, 32] to achieve approximation rates comparable to the benchmark rates given by the Kolmogorov n-widths. In the following sections, which describe the model reduction method, we view the domain U as finite-dimensional, i.e. restricted to the J dimensions that correspond to the current level of truncation. With this in mind, we will use the weight function $\boldsymbol{\pi}(\boldsymbol{y}) = \otimes_{j=1}^{J} \sqrt{\exp(-y_j^2/2)}$ in our formulation of the model reduction methods, i.e. we employ weighted variants of model reduction methods, taking into account *explicitly* the underlying Gaussian measure.

3.2.1. Affine representation by the Empirical Interpolation Method. The parametric representation (2.34) has the disadvantage that is non-linear and therefore non-separable in the spatial and parametric domain. This poses a problem for the efficient application of model reduction methods and in particular for the offline-online decomposition. To overcome this issue, we will employ the (weighted) Empirical Interpolation Method (EIM) (see [9, 57, 45], also [20] for the weighted variant) to achieve an affine approximation for $\sigma_-(\cdot, \boldsymbol{y}) \in$

[1]The Kolmogorov n-width gives a measure of how well a subset K of a normed linear space X can be approximated by n-dimensional subspaces of X. It is defined as

$$d_n(K)_X = \inf_{\substack{X_n \subset X \\ \dim X_n = n}} \sup_{v \in K} \inf_{w \in X_n} \|v - w\|_X. \tag{3.27}$$

The p-average n-width is defined for $K = v(U)$ as

$$\delta_n^{(p)}(K, \mu)_X = \inf_{\substack{X_n \subset X \\ \dim X_n = n}} \left(\int_U \inf_{w \in X_n} \|v - w\|_X^p \, d\mu \right)^{1/p}. \tag{3.28}$$

In our case, for the squared average n-width of $\mathcal{M}$, we can directly use the best n-term Hermite approximation theory from [6] to get the upper bound $\delta_n^{(2)}(\mathcal{M}, \gamma_G)_V \leq K n^{-s}$, with $s = 1/p - 1/2$.

$C(\overline{D}_-), \forall \boldsymbol{y} \in U$, of the form

$$\sigma_-(\boldsymbol{x},\boldsymbol{y}) \approx \mathcal{I}^{\boldsymbol{x}}_{N_I}[\sigma_-(\boldsymbol{x},\boldsymbol{y})] = \sum_{j=1}^{N_I} \xi_j(\boldsymbol{y}) g_j(\boldsymbol{x}), \quad \boldsymbol{x} \in D_-,\ \boldsymbol{y} \in U, \tag{3.29}$$

where $\mathcal{I}^{\boldsymbol{x}}_{N_I}$ is the interpolation operator, with the superscript $\boldsymbol{x}$ denoting that the interpolation is performed in the spatial domain, $(g_j)_{j=1}^{N_I}$ is the nested set of chosen basis functions and $\xi_j(\boldsymbol{y})$ are coefficient functions that are determined by the condition

$$\mathcal{I}^{\boldsymbol{x}}_{N_I}[\sigma_-(\boldsymbol{t^i},\boldsymbol{y})] = \sigma_-(\boldsymbol{t^i},\boldsymbol{y}), \quad i = 1,\dots,N_I, \tag{3.30}$$

for some nested set of chosen points $(\boldsymbol{t^i})_{i=1}^{N_I} \in \overline{D}_-$. This results in the following linear system

$$\sum_{j=1}^{N_I} g_j(\boldsymbol{t}^i)\xi_j(\boldsymbol{y}) = \sigma_-(\boldsymbol{t}^i,\boldsymbol{y}), \quad i = 1,\dots,N_I, \tag{3.31}$$

which can be shown to be uniquely solvable for $N_I \le N_I^{\max} \le \dim(\operatorname{span}\{\mathcal{G}\})$ if one picks the basis functions and points according to the following greedy procedure: choose the first point in U as $\boldsymbol{y}^1 = \arg\sup_{\boldsymbol{y}\in U}\left[\boldsymbol{\pi}(\boldsymbol{y})\|\sigma_-(\cdot,\boldsymbol{y})\|_{L^\infty(D_-)}\right]$ and the first interpolation point as $\boldsymbol{t}^1 = \arg\sup_{\boldsymbol{x}\in\overline{D}_-}|\sigma_-(\boldsymbol{x},\boldsymbol{y}^1)|$. Then define the first basis function as $g_1(\boldsymbol{x}) = \sigma_-(\boldsymbol{x},\boldsymbol{y}^1)/\sigma_-(\boldsymbol{t}^1,\boldsymbol{y}^1)$. The construction of the approximation proceeds at the N_I-th step (until some a priori $N_I = N_I^{\max}$ number of steps or until some tolerance tol_{EIM} is achieved), by choosing the (N_I+1)-th point in U as

$$\boldsymbol{y}^{N_I+1} = \arg\sup_{\boldsymbol{y}\in U}\left[\boldsymbol{\pi}(\boldsymbol{y})\varepsilon^{\sigma_-}_{N_I}(\boldsymbol{y})\right], \tag{3.32}$$

$$\varepsilon^{\sigma_-}_{N_I}(\boldsymbol{y}) = \|\sigma_-(\cdot,\boldsymbol{y}) - \mathcal{I}^{\boldsymbol{x}}_{N_I}\sigma_-(\cdot,\boldsymbol{y})\|_{L^\infty(D_-)}, \tag{3.33}$$

and the (N_I+1)-th interpolation point as

$$\boldsymbol{t}^{N_I+1} = \arg\sup_{\boldsymbol{x}\in\overline{D}_-}|r_{N_I+1}(\boldsymbol{x})|, \tag{3.34}$$

where $r_{N_I+1}(\boldsymbol{x})$ is the residual given by

$$r_{N_I+1}(\boldsymbol{x}) = \sigma_-(\boldsymbol{x},\boldsymbol{y}^{N_I+1}) - \mathcal{I}^{\boldsymbol{x}}_{N_I}\sigma_-(\boldsymbol{x},\boldsymbol{y}^{N_I+1}). \tag{3.35}$$

Then the (N_I+1)-th basis function is obtained by

$$g_{N_I+1}(\boldsymbol{x}) = \frac{r_{N_I+1}(\boldsymbol{x})}{r_{N_I+1}(\boldsymbol{t}^{N_I+1})}. \tag{3.36}$$

We can also define an a posteriori error indicator as

$$\Delta^{\sigma_-}_{N_I}(\boldsymbol{y}) = |\sigma_-(\boldsymbol{t}^{N_I+1},\boldsymbol{y}) - \mathcal{I}^{\boldsymbol{x}}_{N_I}\sigma_-(\boldsymbol{t}^{N_I+1},\boldsymbol{y})|, \tag{3.37}$$

and we can easily see that $\varepsilon_{N_I}^{\sigma_-}(\boldsymbol{y}) \geq \Delta_{N_I}^{\sigma_-}(\boldsymbol{y})$. In practice, the optimization problems (3.32) and (3.34) are replaced by discrete versions over a finite training set $U_{\text{train}} \subset U$ and using a discrete approximation $D_h \subset D_-$, thus relaxing the greedy algorithm to its weak form. We will a priori choose D_h as the nodes of a mesh (the same mesh that we use to solve the Karhunen-Loève eigenvalue problem). However, due to the high-dimensionality of U, we will not a priori choose a training set; instead we will use a collection of training sets that are determined by the SQ algorithm as we detail in subsection 3.3.

Having obtained an affine approximation, the EIM, Hi-Fi, parametric problem becomes: given $\boldsymbol{y} \in U$, find $\boldsymbol{E}_{h,N_I}(\boldsymbol{y}) \in V_h$ such that

$$a_{N_I}(\boldsymbol{E}_{h,N_I}(\boldsymbol{y}), \boldsymbol{v}_h; \sigma(\boldsymbol{y})) = s(\boldsymbol{E}_{h,N_I}(\boldsymbol{y}), \boldsymbol{v}_h) - \imath\omega m(\boldsymbol{E}_{h,N_I}(\boldsymbol{y}), \boldsymbol{v}_h; \sigma_+\chi_{D_+}) - \imath\omega \sum_{k=1}^{N_I} \xi_k(\boldsymbol{y}) m(\boldsymbol{E}_{h,N_I}(\boldsymbol{y}), \boldsymbol{v}_h; g_k\chi_{D_-}) \tag{3.38}$$

$$= f(\boldsymbol{v}_h), \quad \forall \boldsymbol{v}_h \in V_h, \tag{3.39}$$

or in algebraic form

$$\mathrm{A}_{h,N_I}(\boldsymbol{y})\boldsymbol{e}_{h,N_I}(\boldsymbol{y}) = \left(\mathrm{S} - \imath\omega\mathrm{M}_+ - \imath\omega \sum_{k=1}^{N_I} \xi_k(\boldsymbol{y})\mathrm{M}_k\right) \boldsymbol{e}_{h,N_I}(\boldsymbol{y}) = \boldsymbol{b}, \tag{3.40}$$

with

$$(\mathrm{M}_k)_{ij} = m(\boldsymbol{N}_j, \boldsymbol{N}_i; g_k\chi_{D_-}), \quad i,j = 1,\dots,N_h, \quad k = 1,\dots,N_I. \tag{3.41}$$

As we can see, the EIM approximation introduces the sesquilinear form a_{N_I} and we can derive the estimate

$$\|a(\cdot,\cdot;\sigma(\boldsymbol{y})) - a_{N_I}(\cdot,\cdot;\sigma(\boldsymbol{y}))\|_{\mathcal{L}(V_h,V_h^*)} \tag{3.42}$$

$$= \omega \sup_{\boldsymbol{u}_h \in V_h\setminus\{0\}} \sup_{\boldsymbol{v}_h \in V_h\setminus\{0\}} \frac{\left|m\left(\boldsymbol{u}_h, \boldsymbol{v}_h; (\sigma_-(\boldsymbol{y}) - \mathcal{I}_{N_I}^{\boldsymbol{x}}[\sigma_-(\boldsymbol{y})])\chi_{D_-}\right)\right|}{\|\boldsymbol{u}_h\|_V \|\boldsymbol{v}_h\|_V} \tag{3.43}$$

$$\leq \omega\varepsilon_{N_I}^{\sigma_-}(\boldsymbol{y})\gamma_m \tag{3.44}$$

with

$$\gamma_m = \sup_{\boldsymbol{u_h} \in V_h\setminus\{0\}} \sup_{\boldsymbol{v_h} \in V_h\setminus\{0\}} \frac{|m(\boldsymbol{u_h}, \boldsymbol{v_h})|}{\|\boldsymbol{u_h}\|_V \|\boldsymbol{v_h}\|_V} = 1. \tag{3.45}$$

However, this estimate is in most cases pessimistic. In our numerical examples, we will instead use a non-rigorous approach that can be both computationally efficient and efficient as an error estimator. This is obtained as

$$|a(\boldsymbol{u}_h, \boldsymbol{v}_h; \sigma(\boldsymbol{y})) - a_{N_I}(\boldsymbol{u}_h, \boldsymbol{v}_h; \sigma(\boldsymbol{y}))| \tag{3.46}$$

$$= |a(\boldsymbol{u}_h, \boldsymbol{v}_h; \sigma(\boldsymbol{y})) - a_{N_I+N_E}(\boldsymbol{u}_h, \boldsymbol{v}_h; \sigma(\boldsymbol{y})) + a_{N_I+N_E}(\boldsymbol{u}_h, \boldsymbol{v}_h; \sigma(\boldsymbol{y})) - a_{N_I}(\boldsymbol{u}_h, \boldsymbol{v}_h; \sigma(\boldsymbol{y}))| \tag{3.47}$$

$$\lessapprox |a_{N_I+N_E}(\boldsymbol{u}_h, \boldsymbol{v}_h; \sigma(\boldsymbol{y})) - a_{N_I}(\boldsymbol{u}_h, \boldsymbol{v}_h; \sigma(\boldsymbol{y}))| := \delta_{N_I,N_E}^{\alpha}(\boldsymbol{u}_h, \boldsymbol{v}_h; \boldsymbol{y}), \tag{3.48}$$

where N_E denotes a sufficiently high number of terms in an auxiliary EIM approximation such that $|a - a_{N_I+N_E}| \ll |a_{N_I+N_E} - a_{N_I}|$.

3.2.2. Model reduction by the Empirical Interpolation Method-Reduced Basis approximation. We now describe the derivation of a Low-Fi representation of (3.40) using the projection-based (weighted) Reduced Basis method (RB) (see [19] for weighted version). Suppose we have at hand a low-dimensional space $V_{N_P} \subset V_h$, that is spanned by some basis functions $(\boldsymbol{w}_j)_{j=1}^{N_P}$. Then we use the Galerkin RB[2] to obtain the Low-Fi, EIM-RB parametric problem: given $\boldsymbol{y} \in U$, find $\boldsymbol{E}_{N_I,N_P}(\boldsymbol{y}) \in V_{N_P}$ such that

$$a_{N_I}(\boldsymbol{E}_{N_I,N_P}(\boldsymbol{y}), \boldsymbol{v}_{N_P}; \sigma(\boldsymbol{y})) = f(\boldsymbol{v}_{N_P}), \quad \forall \boldsymbol{v}_{N_P} \in V_{N_P}. \tag{3.49}$$

By expressing the reduced basis in terms of the Hi-Fi space basis we get $\boldsymbol{w}_j = \sum_{k=1}^{N_h} w_j^k \boldsymbol{N}_k$ for $j = 1, \dots, N_P$. We arrange the coefficients into the columns of a basis transformation matrix $(\mathrm{W})_{ij} = w_j^i$, with $i = 1, \dots, N_h$ and $j = 1, \dots, N_P$ and we use $\boldsymbol{E}_{N_I,N_P}(\boldsymbol{y}) = \sum_{k=1}^{N_P} e^k_{N_I,N_P}(\boldsymbol{y}) \boldsymbol{w}_k$ to obtain the following Low-Fi, dense linear system

$$\mathrm{A}_{N_I,N_P}(\boldsymbol{y}) \boldsymbol{e}_{N_I,N_P}(\boldsymbol{y}) = \mathrm{W}^H \left(\mathrm{S} - \imath\omega \mathrm{M}_+ - \imath\omega \sum_{k=1}^{N_I} \xi_k(\boldsymbol{y}) \mathrm{M}_k \right) \mathrm{W} \boldsymbol{e}_{N_I,N_P}(\boldsymbol{y}) = \mathrm{W}^H \boldsymbol{b}, \tag{3.50}$$

where W^H denotes the Hermitian conjugate of W. Again, we can store the $\boldsymbol{y}$-independent reduced matrices $\mathrm{W}^H\mathrm{S}\mathrm{W}$, $\mathrm{W}^H\mathrm{M}_+\mathrm{W}$, $\mathrm{W}^H\mathrm{M}_k\mathrm{W}$ and the vector $\mathrm{W}^H\boldsymbol{b}$ and access them when assembling (3.50).

In order to construct a basis for V_{N_P} we use solutions (snapshots) of the Hi-Fi problem at points $(\boldsymbol{y}^n)_{n=1}^{N_P}$ that are chosen iteratively by a greedy algorithm as the most representative samples in some sense for the approximation of $z(\boldsymbol{y})$. Therefore, we have that

$$V_{N_P} = \mathrm{span}\{\boldsymbol{E}_h(\boldsymbol{y}^n), 1 \le n \le N_P\} = \mathrm{span}\{\boldsymbol{w}_n, 1 \le n \le N_P\}, \tag{3.51}$$

where $\boldsymbol{w}_n$ are obtained from $\boldsymbol{E}_h(\boldsymbol{y}^n)$ by Gram-Schmidt orthogonalization with respect to the V inner product. The goal-oriented greedy algorithm starts from an initial parameter value $\boldsymbol{y}^1 = \arg\sup_{\boldsymbol{y}\in U}[\boldsymbol{\pi}(\boldsymbol{y})|z(\boldsymbol{E}_h(\boldsymbol{y}))|]$ and we set $V_1 = \mathrm{span}\{\boldsymbol{E}_h(\boldsymbol{y}^1)\}$, while also initializing the EIM approximation at $\boldsymbol{y}^1$. Then the construction of the RB space and the enrichment of the EIM approximation proceeds at the $N_{I,P}$-th step (until some a priori $N_{I,P} = N_{I,P}^{\max}$ number of steps or until some tolerance $tol_{\text{EIM-RB}}$ is achieved), by choosing the $(N_{I,P}+1)$-th point in U as

$$\boldsymbol{y}^{N_{I,P}+1} = \arg\sup_{\boldsymbol{y}\in U} \left[\boldsymbol{\pi}(\boldsymbol{y}) \varepsilon^z_{N_I,N_P}(\boldsymbol{y}) \right], \tag{3.52}$$

$$\varepsilon^z_{N_I,N_P}(\boldsymbol{y}) = |z(\boldsymbol{E}_h(\boldsymbol{y})) - \hat{z}_{N_I,N_P}(\boldsymbol{y}))|, \tag{3.53}$$

where $\hat{z}_{N_I,N_P}$ is an EIM-RB representation for z. Once $\boldsymbol{y}^{m+1}$ is determined we refine the EIM-RB approximation by enriching the reduced space, setting $V_{N_P+1} = V_{N_P} \oplus \mathrm{span}\{\boldsymbol{E}_h(\boldsymbol{y}^{m+1})\}$ and/or by enriching the EIM approximation at level $N_I + 1$ as in (3.34), (3.36).

[2]A more general approach would be the Petrov-Galerkin RB method, for which the test space is different than the trial space (see e.g. [31]).

In practice, we replace the optimization problem over U with discrete versions over a collection of training sets U_{train} supplied by the adaptive SQ algorithm. Additionally, since the evaluation of $\varepsilon^z_{N_I,N_P}(\boldsymbol{y})$ is expensive (it requires the solution of Hi-Fi problems), we replace it with an a posteriori error indicator $\Delta^z_{N_I,N_P}(\boldsymbol{y})$ such that $\varepsilon^z_{N_I,N_P}(\boldsymbol{y}) \leq \Delta^z_{N_I,N_P}(\boldsymbol{y})$, which we detail in the next section.

3.2.3. Goal-oriented a posteriori error estimator based on primal-dual EIM-RB. We use a definition of $\Delta^z_{N_I,N_P}$ that is based on a goal-oriented primal-dual reduced basis formulation similar to the approach in [42] (see also [59, 45, 31, 22]). For the approximation of the mean of s, we have $z = s$ and we define an associated dual problem as: given $\boldsymbol{y} \in U$, find $\boldsymbol{E}^{\text{du}}(\boldsymbol{y})$ such that

$$a^*(\boldsymbol{E}^{\text{du}}(\boldsymbol{y}), \boldsymbol{v}; \sigma(\boldsymbol{y})) = -\overline{s(\boldsymbol{v})}, \quad \forall \boldsymbol{v} \in V, \tag{3.54}$$

where $a^*(\boldsymbol{u}, \boldsymbol{v}) = \overline{a(\boldsymbol{v}, \boldsymbol{u})}$ is the adjoint sesquilinear form. The Hi-Fi dual problem is given by: find $\boldsymbol{E}^{\text{du}}_h(\boldsymbol{y}) \in V_h$ such that

$$a(\boldsymbol{v}_h, \boldsymbol{E}^{\text{du}}_h(\boldsymbol{y}); \sigma(\boldsymbol{y})) = -s(\boldsymbol{v}_h), \quad \forall \boldsymbol{v}_h \in V_h, \tag{3.55}$$

or in algebraic form by

$$\mathrm{A}^H_h(\boldsymbol{y})\boldsymbol{e}^{\text{du}}_h(\boldsymbol{y}) = -\boldsymbol{c}^H, \tag{3.56}$$

where $\boldsymbol{c}$ is a row vector with components

$$(\boldsymbol{c})_j = s(\boldsymbol{N}_j), \quad j = 1, \ldots, N_h. \tag{3.57}$$

The corresponding EIM Hi-Fi dual problem with solution denoted as $\boldsymbol{E}^{\text{du}}_{h,N_I}$ is defined analogously.

Remark 3.7. We choose to define the dual Hi-Fi problem on the same FEM space as the primal Hi-Fi problem. Thus, we obtain the same matrix $\mathrm{A}_h(\boldsymbol{y})$, a fact that can be exploited when solving the dual Hi-Fi linear systems by e.g. using a factorization of $\mathrm{A}_h(\boldsymbol{y})$ obtained from the primal problem. An alternative is to use different discretisations, adapted to the two problems (see [23] for an analysis in this case).

We now construct a reduced dual space similar to the reduced primal space. Suppose we have at hand the N_D-dimensional dual space $V^{\text{du}}_{N_D} \subset V_h$, that is spanned by the basis functions $(\boldsymbol{w}^{\text{du}}_j)_{j=1}^{N_D}$. If we denote the basis transformation matrix as W_{du}, we obtain the Low-Fi, EIM-RB dual problem: given $\boldsymbol{y}$, find $\boldsymbol{E}_{N_I,N_D}(\boldsymbol{y}) \in V^{\text{du}}_{N_D}$ such that

$$a_{N_I}(\boldsymbol{v}_{N_D}, \boldsymbol{E}^{\text{du}}_{N_I,N_D}(\boldsymbol{y}); \sigma(\boldsymbol{y})) = -s(\boldsymbol{v}_{N_D}), \quad \forall \boldsymbol{v}_{N_D} \in V^{\text{du}}_{N_D}, \tag{3.58}$$

or in algebraic form

$$\left(\mathrm{A}^{\text{du}}_{N_I,N_D}(\boldsymbol{y})\right)^H \boldsymbol{e}^{\text{du}}_{N_I,N_D}(\boldsymbol{y}) = \mathrm{W}^H_{\text{du}} \left(\mathrm{S} - \imath\omega\mathrm{M}_+ - \imath\omega \sum_{k=1}^{N_I} \xi_k(\boldsymbol{y})\mathrm{M}_k\right)^H \mathrm{W}_{\text{du}}\boldsymbol{e}^{\text{du}}_{N_I,N_D}(\boldsymbol{y}) = -\mathrm{W}^H_{\text{du}}\boldsymbol{c}^H, \tag{3.59}$$

where we used the expansion $\boldsymbol{E}^{\rm du}_{N_I,N_D}(\boldsymbol{y}) = \sum_{k=1}^{N_D} e^k_{N_I,N_D}(\boldsymbol{y})\boldsymbol{w}^{\rm du}_k$. The construction of $V^{du}_{N_D}$ proceeds as in the primal problem by using solutions of (3.56) for the selected $\boldsymbol{y}$. To specify the a posteriori error indicator, we first need to define the primal residual as

$$r^{\rm pr}_{N_I,N_P}(\boldsymbol{v};\boldsymbol{y}) = f(\boldsymbol{v}) - a_{N_I}(\boldsymbol{E}_{N_I,N_P}(\boldsymbol{y}),\boldsymbol{v};\sigma(\boldsymbol{y})), \quad \forall \boldsymbol{v}\in V, \tag{3.60}$$

and the dual residual as

$$r^{\rm du}_{N_I,N_D}(\boldsymbol{v};\boldsymbol{y}) = -s(\boldsymbol{v}) - a_{N_I}(\boldsymbol{v},\boldsymbol{E}^{\rm du}_{N_I,N_D}(\boldsymbol{y});\sigma(\boldsymbol{y})), \quad \forall \boldsymbol{v}\in V. \tag{3.61}$$

We also denote the primal and dual EIM-RB errors as $\boldsymbol{\varepsilon}_{N_I,N_P} = \boldsymbol{E}_h - \boldsymbol{E}_{N_I,N_P} \in V_h$ and $\boldsymbol{\varepsilon}^{\rm du}_{N_I,N_D} = \boldsymbol{E}^{\rm du}_h - \boldsymbol{E}^{\rm du}_{N_I,N_D} \in V_h$ respectively. The EIM-RB, dual-corrected representation of $z = s$ is defined as

$$\hat{z}^s_{N_I,N_P,N_D}(\boldsymbol{y}) := \hat{s}_{N_I,N_P,N_D}(\boldsymbol{y}) = s(\boldsymbol{E}_{N_I,N_P}(\boldsymbol{y})) - r^{\rm pr}_{N_I,N_P}(\boldsymbol{E}^{\rm du}_{N_I,N_D};\boldsymbol{y}), \tag{3.62}$$

i.e. we add a correction term that exploits the additional information that the dual problem is providing, leading to sharper error bounds. Using standard arguments, we have the (non-rigorous) error estimate

$$\|\boldsymbol{\varepsilon}_{N_I,N_P}(\boldsymbol{y})\|_V \le \Delta^{\boldsymbol{E}}_{N_I,N_P}(\boldsymbol{y}) := \Delta^{\boldsymbol{E}}_{\rm EIM}(\boldsymbol{y}) + \Delta^{\boldsymbol{E}}_{\rm RB}(\boldsymbol{y}), \tag{3.63}$$

with

$$\Delta^{\boldsymbol{E}}_{\rm EIM} := \frac{\|\delta^a_{N_I,N_E}(\boldsymbol{E}_{N_I,N_P},\cdot;\boldsymbol{y})\|_{V_h^*}}{\alpha_h(\boldsymbol{y})}, \quad \Delta^{\boldsymbol{E}}_{\rm RB} := \frac{\|r^{\rm pr}_{N_I,N_P}(\cdot;\boldsymbol{y})\|_{V_h^*}}{\alpha_h(\boldsymbol{y})}, \tag{3.64}$$

where $\alpha_h(\boldsymbol{y})$ is the (best) discrete coercivity factor given by

$$\alpha_h(\boldsymbol{y}) = \inf_{\boldsymbol{v_h}\in V_h} \frac{|a(\boldsymbol{v_h},\boldsymbol{v_h};\sigma(\boldsymbol{y}))|}{\|\boldsymbol{v_h}\|^2_V}. \tag{3.65}$$

Using an analogous expression for the dual error, we can derive (see Appendix D, also [42]) the following error estimate and corresponding a posteriori estimator $\Delta^s_{N_I,N_P,N_D}$

$$|s(\boldsymbol{E}_h(\boldsymbol{y})) - \hat{z}^s_{N_I,N_P,N_D}(\boldsymbol{y})| \le \Delta^s_{N_I,N_P,N_D}(\boldsymbol{y}) := \alpha_h(\boldsymbol{y})\Delta^{\boldsymbol{E}}_{N_I,N_P}(\boldsymbol{y})\Delta^{\boldsymbol{E}^{\rm du}}_{N_I,N_D}(\boldsymbol{y}) \tag{3.66}$$

$$+ \delta^a_{N_I,N_E}(\boldsymbol{E}_{N_I,N_P},\boldsymbol{E}^{\rm du}_{N_I,N_D};\boldsymbol{y}). \tag{3.67}$$

For the estimation of the covariance and pseudo-covariance of s, we require the approximation of the non-linear quantities $z = s^2$ and $z = |s|^2$ respectively. We therefore introduce an additional dual problem (related to the Fréchet derivative of z) as in [42]: given $\boldsymbol{y}\in U$, find $\boldsymbol{E}^{\rm du2}(\boldsymbol{y})$ such that

$$a^*(\boldsymbol{E}^{\rm du2}(\boldsymbol{y}),\boldsymbol{v};\sigma(\boldsymbol{y})) = -2\overline{\hat{s}_{N_I,N_P,N_D}(\boldsymbol{y})s(\boldsymbol{v})}, \quad \forall \boldsymbol{v}\in V. \tag{3.68}$$

Using analogous definitions for the corresponding Hi-Fi, EIM and EIM-RB problems (employing a reduced space $V^{\rm du2}_{N_{D2}}$ of dimension N_{D2}) and the residual and error, we define the EIM-RB, dual-corrected approximation $\hat{z}^{s^2}$ of s^2 to be

$$\hat{z}^{s^2}_{N_I,N_P,N_D,N_{D2}}(\boldsymbol{y}) = s(\boldsymbol{E}_{N_I,N_P}(\boldsymbol{y}))^2 - \left(r^{\rm pr}_{N_I,N_P}(\boldsymbol{E}^{\rm du}_{N_I,N_D};\boldsymbol{y})\right)^2 - r^{\rm pr}_{N_I,N_P}(\boldsymbol{E}^{\rm du2}_{N_I,N_{D2}};\boldsymbol{y}). \tag{3.69}$$

The following error estimate for the EIM-RB approximation $\hat{z}^{s^2}$ of s^2 and the a posteriori indicator $\Delta^{s^2}_{N_I,N_P,N_D,N_{D2}}$ can be derived similarly to the derivation in Appendix D

$$\left|s(\boldsymbol{E}_h(\boldsymbol{y}))^2 - \hat{z}^{s^2}_{N_I,N_P,N_D,N_{D2}}(\boldsymbol{y})\right| \leq \Delta^{s^2}_{N_I,N_P,N_D,N_{D2}}(\boldsymbol{y}) \tag{3.70}$$

$$:= \left(\Delta^{s}_{N_I,N_P,N_D}(\boldsymbol{y})\right)^2 + \alpha_h(\boldsymbol{y})\Delta^{\boldsymbol{E}}_{N_I,N_P}(\boldsymbol{y})\Delta^{\boldsymbol{E}^{\mathrm{du2}}}_{N_I,N_{D2}}(\boldsymbol{y}) \tag{3.71}$$

$$+ \delta^{a}_{N_I,N_E}(\boldsymbol{E}_{N_I,N_P}, \boldsymbol{E}^{\mathrm{du2}}_{N_I,N_{D2}}; \boldsymbol{y}). \tag{3.72}$$

For the estimation of the covariance of s, we have $z = |s|^2$, so we use instead the following dual problem: given $\boldsymbol{y} \in U$, find $\boldsymbol{E}^{\mathrm{du3}}(\boldsymbol{y})$ such that

$$a^*(\boldsymbol{E}^{\mathrm{du3}}(\boldsymbol{y}), \boldsymbol{v}; \sigma(\boldsymbol{y})) = -2\hat{s}_{N_I,N_P,N_D}(\boldsymbol{y})\overline{s(\boldsymbol{v})}, \quad \forall \boldsymbol{v} \in V. \tag{3.73}$$

Then we define the EIM-RB, dual-corrected approximation $\hat{z}^{|s|^2}$ of $|s|^2$ to be

$$\hat{z}^{|s|^2}_{N_I,N_P,N_D,N_{D3}}(\boldsymbol{y}) = |s(\boldsymbol{E}_{N_I,N_P}(\boldsymbol{y}))|^2 - \left|r^{\mathrm{pr}}_{N_I,N_P}(\boldsymbol{E}^{\mathrm{du}}_{N_I,N_D}; \boldsymbol{y})\right|^2 - \Re\left(r^{\mathrm{pr}}_{N_I,N_P}(\boldsymbol{E}^{\mathrm{du3}}_{N_I,N_{D3}}; \boldsymbol{y})\right). \tag{3.74}$$

The error estimate for the EIM-RB approximation $\hat{z}^{|s|^2}$ of $|s|^2$ and the a posteriori indicator $\Delta^{|s|^2}_{N_I,N_P,N_D,N_{D3}}$ are expressed as follows

$$\left||s(\boldsymbol{E}_h(\boldsymbol{y}))|^2 - \hat{z}^{|s|^2}_{N_I,N_P,N_D,N_{D3}}(\boldsymbol{y})\right| \leq \Delta^{|s|^2}_{N_I,N_P,N_D,N_{D3}}(\boldsymbol{y}) \tag{3.75}$$

$$:= \left(\Delta^{s}_{N_I,N_P,N_D}(\boldsymbol{y})\right)^2 + \alpha_h(\boldsymbol{y})\Delta^{\boldsymbol{E}}_{N_I,N_P}(\boldsymbol{y})\Delta^{\boldsymbol{E}^{\mathrm{du3}}}_{N_I,N_{D3}}(\boldsymbol{y}) \tag{3.76}$$

$$+ \delta^{a}_{N_I,N_E}(\boldsymbol{E}_{N_I,N_P}, \boldsymbol{E}^{\mathrm{du3}}_{N_I,N_{D3}}; \boldsymbol{y}). \tag{3.77}$$

Note that instead of constructing two different reduced dual spaces for problems (3.68) and (3.73), we can instead approximately use only the RB space constructed from (3.68), so that the EIM-RB solutions are related as $\boldsymbol{E}^{\mathrm{du3}}_{N_I,N_{D3}} = \boldsymbol{E}^{\mathrm{du2}}_{N_I,N_{D2}}\hat{s}_{N_I,N_P,N_D}/\overline{\hat{s}_{N_I,N_P,N_D}}$ and $\Delta^{|s|^2}_{N_I,N_P,N_D,N_{D3}} = \Delta^{s^2}_{N_I,N_P,N_D,N_{D2}}$.

In general, we can compute $\alpha_h(\boldsymbol{y})$ as the square root of the minimum eigenvalue $\lambda_{\min}(\boldsymbol{y})$ of the generalized eigenvalue problem $\mathrm{A}_h^H(\boldsymbol{y})\mathrm{X}_h^{-1}\mathrm{A}_h(\boldsymbol{y})\mathbf{v} = \lambda(\boldsymbol{y})\mathrm{X}_h\mathbf{v}$, where X_h is the discrete representation of the V inner product in the FEM basis. However, this computation involves Hi-Fi operations and therefore we cannot use it for the efficient online evaluation of the a posteriori error indicator. We rely instead on an approximation of $\alpha_h(\boldsymbol{y})$ which we describe in the next section 3.2.4.

With regard to the computation of the dual norms of the primal and dual residuals and of other required linear or anti-linear forms such as $\delta^{a}_{N_I,N_E}(\boldsymbol{E}_{N_I,N_P}, \cdot; \boldsymbol{y})$, this can be efficiently achieved through an offline-online decomposition using the corresponding Riesz representatives (see e.g. [57, 59]). For the primal residual, we use the Riesz representative $\widehat{\boldsymbol{r}}^{\mathrm{pr}}_{N_I,N_P}(\boldsymbol{y}) \in V_h$, so that $\|r^{\mathrm{pr}}_{N_I,N_P}(\cdot; \boldsymbol{y})\|^2_{V_h^*} = \|\widehat{\boldsymbol{r}}^{\mathrm{pr}}_{N_I,N_P}(\boldsymbol{y})\|^2_V$. Then using the notation $\mathrm{A}_0 = (\mathrm{S} - \imath\omega\mathrm{M}_+)$ and

$\mathrm{A_k} = -\imath\omega \mathrm{M}_k$ and setting $\xi_0 = 1$, we get

$$\|\widehat{\boldsymbol{r}}^{\mathrm{pr}}_{N_I,N_P}(\boldsymbol{y})\|^2_V = \boldsymbol{b}^H \mathrm{X}_h^{-1}\boldsymbol{b} \tag{3.78}$$

$$- 2\Re\left(\sum_{i=0}^{N_I} \xi_i(\boldsymbol{y}) \boldsymbol{e}^H_{N_I,N_P}(\boldsymbol{y}) \mathrm{W}^H \mathrm{A}_i^H \mathrm{X}_h^{-1}\boldsymbol{b}\right) \tag{3.79}$$

$$+ \sum_{i,j=0}^{N_I} \xi_i(\boldsymbol{y})\xi_j(\boldsymbol{y}) \boldsymbol{e}^H_{N_I,N_P}(\boldsymbol{y}) \mathrm{W}^H \mathrm{A}_i^H \mathrm{X}_h^{-1} \mathrm{A}_j \mathrm{W} \boldsymbol{e}_{N_I,N_P}(\boldsymbol{y}), \tag{3.80}$$

where $\boldsymbol{y}$-independent quantities can be stored in the offline phase. An expression for the dual norms of other quantities can be derived analogously.

Remark 3.8. We choose to enrich the dual spaces simultaneously with the primal space (i.e. $N_P = N_D = N_{D2} = N_{D3}$) for the $\boldsymbol{y}^{m+1}$ that are selected at the m-th step by the greedy algorithm, using the weighted a posteriori error indicator $\boldsymbol{\pi}(\boldsymbol{y})\Delta^z$, where Δ^z denotes the appropriate error indicator for the specific z. Therefore, in this approach, the dimensions of all reduced spaces grow at the same rate. Essentially, this reflects the estimate that the Kolmogorov n-widths of the primal and dual problems decay at approximately the same rate. In cases where the decay rate of one problem is significantly faster, the growth of the corresponding reduced space is more important for fast convergence of $|z - \hat{z}|$ (for a more thorough discussion see [31]).

3.2.4. Coercivity constant approximation by Radial Basis Function interpolation. Generally in RB, the Successive Constraint Method (SCM) [48] can be used to obtain lower bounds on $\alpha_h(\boldsymbol{y})$ and enable the fast evaluation of the posteriori error indicator (see also [44] for a comparison of different approaches). However, due to the computational effort required for SCM in high dimensions and our use of adaptive training sets, we rely instead on a heuristic approximation $\alpha_I(\boldsymbol{y})$ of $\alpha_h(\boldsymbol{y})$, achieved through a Radial Basis Function (RBF) interpolation as proposed in [52]. For a training set $(\boldsymbol{y}^k)_{k=1}^{N_t} = U_{\mathrm{train}} \subset U$ and truncation level J, we build the RBF interpolant $\alpha_I(\boldsymbol{y}) > 0$ by computing the coercivity constant $\alpha_h(\boldsymbol{y})$ for each $\boldsymbol{y} \in U_{\mathrm{train}}$ and defining

$$\log \alpha_I(\boldsymbol{y}) = \beta_0 + \sum_{j=1}^{J} \beta_j y_j + \sum_{k=1}^{N_t} \gamma_k \varphi(|\boldsymbol{y} - \boldsymbol{y}_k|), \tag{3.81}$$

where $\varphi(r) = e^{-r^2}$ is the RBF and γ_k are weights that satisfy the relations

$$\log \alpha_I(\boldsymbol{y}) = \log \alpha_h(\boldsymbol{y}), \quad \forall \boldsymbol{y} \in U_{\mathrm{train}}, \tag{3.82}$$

$$\sum_{k=1}^{N_t} \gamma_k = 0, \quad \sum_{k=1}^{N_t} \gamma_k (\boldsymbol{y}^k)_j, \quad j = 1, \ldots, J. \tag{3.83}$$

The resulting system is solved in the offline phase for the weights β_j, $j = 0, \ldots, J$ and γ_k, $k = 1, \ldots, N_t$. Then, in the online phase, we compute the RBF approximation from (3.81). Similar to the EIM and RB methods, we don't choose a priori a training set but we start from one point $\boldsymbol{y}^1$ and then we progressively add the point $\boldsymbol{y}^m$ to the training set whenever a Hi-Fi solution at $\boldsymbol{y}^m$ is computed.

3.3. Dimension-adaptive SQ-EIM-RB algorithm. In this section we describe the dimension-adaptive Sparse Quadrature, Empirical Interpolation Method and Reduced Basis algorithm, adapted and extended from ideas in the algorithms presented in [22, 18, 21] and [55]. Algorithm 1 is used for the estimation of the mean of s. Similar algorithms are also used for the estimation of the covariance and pseudo-covariance of s by replacing the error estimators with the appropriate choices.

As it can be seen, the heuristic idea in Algorithm 1 is the replacement of the Hi-Fi model by the EIM-RB reduced model in all SQ operations and the "training" of EIM-RB over a collection of adaptive training sets U_{train}, which are determined by the dimension-adaptive SQ algorithm. For non-nested quadrature rules, these sets are constructed in each iteration as the union of tensor product grids $G_{\boldsymbol{\mu}}$ associated to selected indices $\boldsymbol{\mu}$. For nested rules we can instead consider only the new points added to the grid by each selected index $\boldsymbol{\mu}$. By performing this adaptive procedure, we aim to capture with specified accuracy the behaviour of the Hi-Fi model across the parametric dimensions that are most important for the estimation of the QoI. At each step, we estimate the EIM-RB approximation error $\mathcal{E}_{\text{EIM-RB}}(\boldsymbol{y}) = \boldsymbol{\pi}(\boldsymbol{y})\Delta^{z}_{N_I,N_P,N_D}(\boldsymbol{y})$ and refine the EIM or/and the RB approximations when needed, based on corresponding error contributions which are estimated to be given by

$$\mathcal{E}_{\text{EIM}}(\boldsymbol{y}) = \boldsymbol{\pi}(\boldsymbol{y})\alpha_I(\boldsymbol{y})\Delta^{\boldsymbol{E}}_{\text{EIM}}(\boldsymbol{y})\Delta^{\boldsymbol{E}^{\text{du}}}_{\text{EIM}}(\boldsymbol{y}), \tag{3.84}$$

and

$$\mathcal{E}_{\text{RB}}(\boldsymbol{y}) = \boldsymbol{\pi}(\boldsymbol{y})\alpha_I(\boldsymbol{y})\Delta^{\boldsymbol{E}}_{\text{RB}}(\boldsymbol{y})\Delta^{\boldsymbol{E}^{\text{du}}}_{\text{RB}}(\boldsymbol{y}), \tag{3.85}$$

respectively. If we assume all error contributions to be balanced and the error estimators to be effective, then we can estimate that to achieve a tolerance $tol_{\text{EIM-RB}}$ for $\mathcal{E}_{\text{EIM-RB}}$, we can set $tol_{\text{EIM}} \simeq tol_{\text{RB}} \simeq tol_{\text{EIM-RB}}/c$ for $\mathcal{E}_{\text{RB}}$ and $\mathcal{E}_{\text{EIM}}$, for some constant $c > 1$. The choice of the tolerance $tol_{\text{EIM-RB}}$ is crucial for the performance of the algorithm and it should be selected low enough such that SQ error converges to the desired accuracy but not too low as this would make the model reduction inefficient. Of course, the efficiency of the error estimator, defined as the ratio of the estimator to the actual error plays an important role and we would like this to be as close to unity as possible.

Remark 3.9. Note that the algorithm requires the exploration of the reduced margin R_Λ of Λ. Since in general we wouldn't want to discard function evaluations, the output can be considered to be the index set $\tilde{\Lambda} = \Lambda \cup R_\Lambda$ and the associated quadrature. The theoretical estimate however does indeed refer to the index set Λ since this captures (heuristically) the largest contributions.

3.3.1. Computational complexity. We give here a short description of the computational complexity involved in the elements in Algorithm 1 for the case $z = s$. First, if we assume that we require N_{SQ} Hi-Fi solutions (each involving the solution of a system with N_h degrees of freedom) to achieve a specified accuracy ϵ using a SQ-only version of the algorithm, then the computational complexity in this case scales dominantly as $O(N_{SQ}N_h^p)$ (complex) operations, where $p \leq 3$ depends on the solver used and the sparsity of the matrices involved. In the case of the SQ-EIM-RB algorithm, the situation is more complex as we have to take

into account the computational work involved in both training and evaluating the Low-Fi approximation. This is usually split into an "offline" and "online" phase; in our case the two phases interchange due to the adaptive nature of the algorithm. For our purposes, "offline" phase consists of enriching the Low-Fi approximations and updating the required reduced quantities. On the other hand, the "online" phase consists of evaluating the a posteriori error estimators and calculating the Low-Fi approximations. For reasonable values of N_P and N_I the "online" phase is computationally less costly than the "offline" phase so we focus on the second. If we assume that to achieve an accuracy ϵ, the algorithm requires N_I terms for the EIM approximation and a size of $N_P = N_D$ for the RB spaces, then the computational cost in total for the "offline" phases is dominated by: i) the solution of the primal Hi-Fi systems which scales as $O(N_P N_h^p)$ (note that we assume a factorization is obtained from the primal problems and used to solve the dual problems, thus making the associated computational work negligible), ii) the solution of the generalized eigenvalue problems which scales as $O(N_P N_h^{p'})$ for some p' possibly different than p and iii) the computation required for the a posteriori error estimation which has cost that depends on the current values of N_I, N_E, N_P, N_h at each update of the offline quantities. For this last contribution we can give a rough estimate of cost as $O\left(4(2N_I + N_E)N_P N_h^2 + 4(N_I^2 + (N_I + N_E)^2)N_P^2 N_h\right)$ for the current values of N_I, N_E, N_P at each update, where we assumed that in the Hi-Fi dimension N_h, the cost of solving a factorized system and the cost of a matrix-vector product, is $2N_h^2$ operations. Depending on N_h and the required N_P, N_I, N_E, a plain SQ or a SQ-EIM-RB approach is computationally less costly, for example as N_h gets large the cost of solving the Hi-Fi systems dominates and the model reduction approach performs favourably.

4. Numerical experiment. In this section we present numerical evidence to showcase the performance of our method. Let us mention that we use our own MATLAB® [53] implementations of FEM (with efficient assembly of forms as in [58]) and of the EIM-RB method. For SQ we make use of the sparse grids MATLAB kit [8] with suitable modifications.

The model and the parameters in Maxwell equations are chosen to represent a typical low-frequency ($f = 1$) CSEM survey. We set $\mu = \mu_0$, $\omega = 2\pi$ and $\|\boldsymbol{p}_s\|_2 = 50000$. The domain is $D = (-5000, 5000) \times (-5000, 5000) \times (-4000, 4000)$, which is separated into D_+ (the sea layer) and D_- (the subsurface) by the horizontal plane $z = 0$. Figure 4.1(b) shows a horizontal slice of the tetrahedral mesh used in our examples, which is a priori refined at the regions around the source $\boldsymbol{x}_s = (-500, -350, 300)$ and sensor $\boldsymbol{x}_r = (300, 450, 200)$ positions, while it is coarser near the boundary. The total number of tetrahedra amounts to $n_c = 62786$ which results in $N_h = 70284$ internal degrees of freedom for the Hi-Fi FEM problems, that are solved using the sparse direct solver MUMPS [3]. As mentioned in section 2.2.2, we use a regularization for point sources that has spherically symmetric components. We use an x-oriented source and receiver and we set $\boldsymbol{j}_H = \|\boldsymbol{p}_s\|_2 (j_H^1, 0, 0)$ with

$$j_H^1 = \begin{cases} \frac{1}{H^3}\eta_{m,p}(r/H) & r \le H, \\ 0 & r > H, \end{cases} \tag{4.1}$$

where $r = \|\boldsymbol{x} - \boldsymbol{x}_s\|_2$ and $\eta_{m,p}(r)$ is a polynomial of degree p in the ball $B(0,1)$ that is expressed in terms of the shifted Legendre polynomials and satisfies the compact m-moment conditions together with suitable continuity conditions. In our experiments we use $\eta_{2,3}(r) =$

Algorithm 1: Dimension-adaptive SQ-EIM-RB algorithm

Input: tolerances tol, tol_{EIM}, tol_{RB}, $tol_{\text{EIM-RB}}$, maximum cardinality $N^{\max}$, starting truncation level J, N_E, map $z(\boldsymbol{y}) = s(\boldsymbol{E}(\boldsymbol{y}))$;

Output: index sets Λ_N, $\tilde{\Lambda}_N = \Lambda_N \cup R_{\Lambda_N}$, quadratures $\mathcal{Q}_{\Lambda_N}[z]$, $\mathcal{Q}_{\tilde{\Lambda}_N}[z]$;

Initialize: $N = N_P = N_I = 1, \boldsymbol{\nu} = \mathbf{0}, \Lambda_N = \tilde{\Lambda}_N = \{\mathbf{0}\}, R_{\Lambda_N} = \{\varnothing\}, A = \mathbf{0}, \mathcal{E} = 2 \cdot tol$;

a) construct initial sparse grid G_{Λ_N} from (3.7);

b) solve the primal and dual Hi-Fi problems at G_{Λ_N};

c) construct initial EIM-RB primal and dual spaces, initialize auxiliary EIM with N_E terms at random points, store offline quantities, initialize RBF approximation (3.81);

d) calculate initial SQ approximation $Q_{old} = \mathcal{Q}_{\Lambda_N}[z]$ as in (3.8);

while $N < N^{\max}$ ***and*** $\mathcal{E} > tol$ **do**

  find $N(\boldsymbol{\nu}, \Lambda_N)$ as in (3.19), $U_{\text{train}} = \{\varnothing\}$;

  for $\boldsymbol{\mu} \in N(\boldsymbol{\nu}, \Lambda_N)$ ***and*** $\Lambda_N \cup \{\boldsymbol{\mu}\}$ *is downward closed* **do** $U_{\text{train}} = U_{\text{train}} \cup G_{\boldsymbol{\mu}}$;

  `// Train EIM-RB on` $U_{\texttt{train}}$

  find $\boldsymbol{y}^{N_{I,P}+1} = \arg\sup_{\boldsymbol{y} \in U_{\text{train}}} \left[\boldsymbol{\pi}(\boldsymbol{y}) \Delta^z_{N_I,N_P,N_D}(\boldsymbol{y})\right]$, $N_{\text{train}} = 0$;

  while $\mathcal{E}_{EIM\text{-}RB}(\boldsymbol{y}^{N_{I,P}+1}) > tol_{EIM\text{-}RB}$ ***and*** $N_{train} < \#(U_{train})$ **do**

    if $\mathcal{E}_{EIM}(\boldsymbol{y}^{N_{I,P}+1}) > tol_{EIM}$ **then**

      enrich main and auxiliary EIM approximations at $\boldsymbol{y}^{N_{I,P}+1}$, $N_I = N_I + 1$;

    end

    if $\mathcal{E}_{RB}(\boldsymbol{y}^{N_{I,P}+1}) > tol_{RB}$ **then**

      solve primal and dual Hi-Fi problems at $\boldsymbol{y}^{N_{I,P}+1}$, enrich spaces;

      $N_P = N_P + 1$, add $\alpha_h(\boldsymbol{y}^{N_{I,P}+1})$ to RBF approximation;

    end

    update offline quantities, find $\boldsymbol{y}^{N_{I,P}+1} = \arg\sup_{\boldsymbol{y} \in U_{\text{train}}} \left[\boldsymbol{\pi}(\boldsymbol{y}) \Delta^z_{N_I,N_P,N_D}(\boldsymbol{y})\right]$;

    $N_{\text{train}} = N_{\text{train}} + 1$;

  end

  for $\boldsymbol{\mu} \in N(\boldsymbol{\nu}, \Lambda_N)$ ***and*** $\Lambda_N \cup \{\boldsymbol{\mu}\}$ *is downward closed* **do**

    $\tilde{\Lambda}_N = \tilde{\Lambda}_N \cup \{\boldsymbol{\mu}\}$, $R_{\Lambda_N} = R_{\Lambda_N} \cup \{\boldsymbol{\mu}\}$;

    evaluate $Q_{\tilde{\Lambda}_N}[z]$ using EIM-RB approximation $\hat{z}_{N_I,N_P,N_D}$;

    compute profit $P(\boldsymbol{\mu}) = (Q_{\tilde{\Lambda}_N} - Q_{\text{old}})[z]$, $Q_{\text{old}} = Q_{\tilde{\Lambda}_N}$;

  end

  choose $\boldsymbol{\tau}$ from R_{Λ_N} with the highest profit and set $\boldsymbol{\nu} = \boldsymbol{\tau}$;

  `// Check for dimension activation`

  if $\exists j = 1, \ldots, J$ ***such that*** $A_j = 0$ ***and*** $\tau_j > 0$ **then**

    $A_j = 1$, $J = J + 1$, $\tilde{\Lambda}_N = \tilde{\Lambda}_N \cup \{\boldsymbol{e}_J\}$, $R_{\Lambda_N} = R_{\Lambda_N} \cup \{\boldsymbol{e}_J\}$;

    train EIM-RB on $U_{\text{train}} = G_{\boldsymbol{e}_J}$ as in 5-16;

    compute profit $P(\boldsymbol{e}_J) = (Q_{\tilde{\Lambda}_N} - Q_{\text{old}})[z]$, $Q_{\text{old}} = Q_{\tilde{\Lambda}_N}$;

    $\boldsymbol{\nu} = \arg\max\left[\max(P(\boldsymbol{\tau}), P(\boldsymbol{e}_J))\right]$;

  end

  $\Lambda_{N+1} = \Lambda_N \cup \{\boldsymbol{\nu}\}, R_{\Lambda_{N+1}} = R_{\Lambda_N} \backslash \{\boldsymbol{\nu}\}$, $\tilde{\Lambda}_{N+1} = \tilde{\Lambda}_N$, $\mathcal{E} = P(\boldsymbol{\nu})$, $N = N + 1$;

end

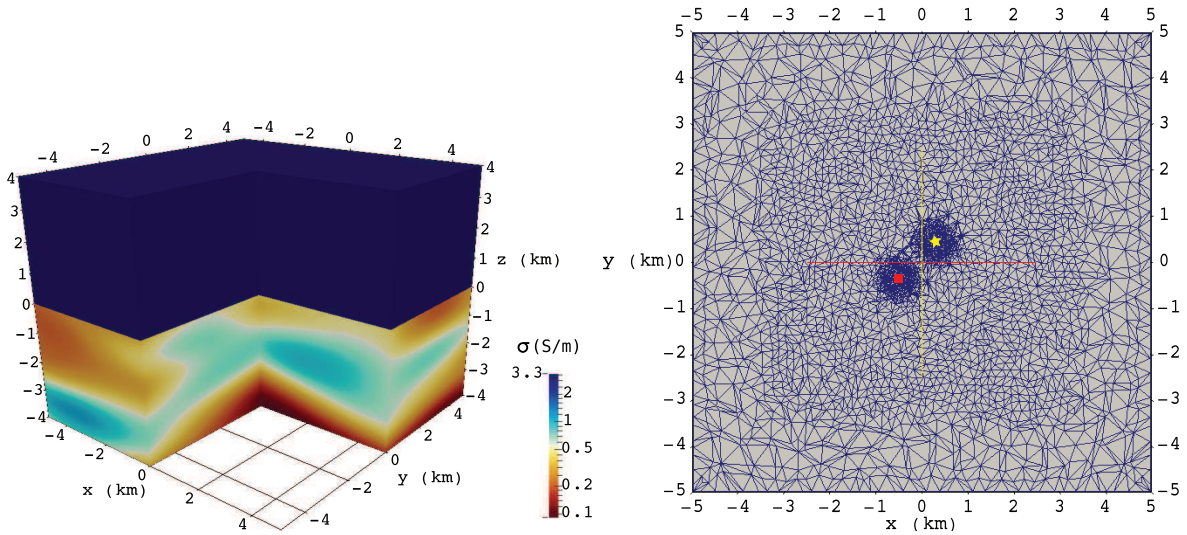

(a) (b)

Figure 4.1: (a) Realization of conductivity random field σ with $\sigma_+ = 3.3$, $\sigma_* = 0$, $\sigma_0 = 1/2$, $\mathrm{Var}[q] = 1$ and Whittle-Matérn covariance function with $\nu = 15/2$ and $M^{1/2} = \mathrm{diag}(1250, 1250, 300)$. (b) Horizontal slice ($z = 150$) of the mesh used in Experiment 1 with $n_c = 62786$ cells, refined at the source (depicted with red square) $\boldsymbol{x}_s = (-500, -350, 300)$ and receiver (depicted with yellow star) $\boldsymbol{x}_r = (300, 450, 200)$ positions.

$-15(-11 + 42 - 51r^2 + 20r^3)/2\pi$, which satisfies the 2-moment conditions and has continuity C^0. A similar representation can be used for the receiver.

4.1. SQ algorithm. For our numerical experiment, we set $\sigma_+ = 3.3$, $\mathrm{Var}[q] = 1$, $\sigma_*(\boldsymbol{x}) = 0$ and $\sigma_0(\boldsymbol{x}) = 1/2$. The smoothness parameter is chosen to be $\nu = 15/2$, which according to the analysis in section 3.1.1 should theoretically lead to a convergence rate $O(N^{-1})$. We use the weight matrix $M^{1/2} = \mathrm{diag}(1250, 1250, 300)$ for the weighted Euclidean norm to account for anisotropy in the z direction. A realization of the conductivity random field is depicted in Figure 4.1(a), while Figure 4.2(a) shows the decay of the normalized eigenvalues λ_j and norms $\|\psi_j\|_{L^\infty(D_-)}$ for this choice of covariance function, which agrees with the theoretical estimates. We start from $J = 10$ dimensions, which capture about 85% of the variance in the KL expansion. As a first test, we employ Algorithm 1 for the approximation of $\mathbb{E}[f]$ with $f(\boldsymbol{y}) = s(\boldsymbol{y}) = s(\boldsymbol{E}(\boldsymbol{y})) = \boldsymbol{e}_x \cdot \delta_{\boldsymbol{x}_r}(\boldsymbol{E}(\boldsymbol{y})) = E_x(\boldsymbol{x}_r; \boldsymbol{y})$, $f(\boldsymbol{y}) = s(\boldsymbol{y})^2$, $f(\boldsymbol{y}) = |s(\boldsymbol{y})|^2$, using a separate simulation for each choice of f. We set the tolerance as $tol = 10^{-5} \cdot |Q_{\Lambda_1}[f]| \approx 4 \cdot 10^{-6}$. We set the tolerance as $tol = 10^{-5} \cdot |Q_{\Lambda_1}[f]| \approx 4 \cdot 10^{-6}$. Approximating the "true" value of the integrals as $E[f] \approx Q_{\tilde{\Lambda}_{400}}[f]$ (see Table 4.2), we report the convergence of the relative error with respect to the number of indices in Figure 4.2(b). The results show a convergence ratio that is in agreement with the theoretical estimate, although the decrease of the error is not monotonic. Note that convergence is observed even for the non-holomorphic function $f = |s|^2$. The computational effort required for $N = 400$ amounts

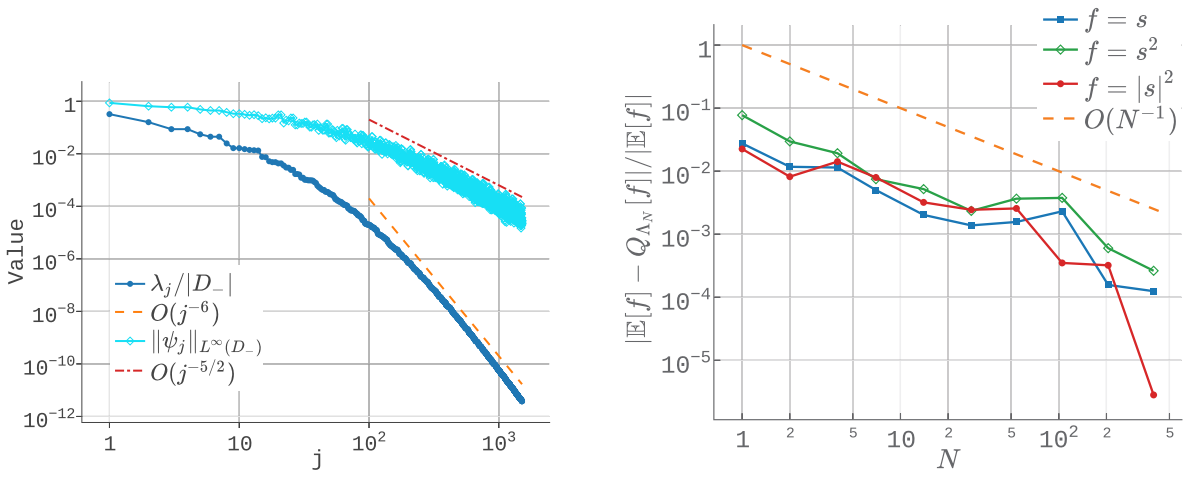

(a) (b)

Figure 4.2: (a) Normalized eigenvalues λ_j and norms $\|\psi_j\|_{L^\infty(D_-)}$ for Whittle-Matérn covariance function with $\nu = 15/2$ and $M^{1/2} = \text{diag}(1250, 1250, 300)$. (b) Convergence of relative error $|\mathbb{E}[f] - Q_{\Lambda_N}[f]|/|\mathbb{E}[f]|$ with respect to the number of indices N for the plain SQ algorithm with $f = s, f = s^2$ and $f = |s|^2$. The "true" value is approximated as $\mathbb{E}[f] \approx Q_{\tilde{\Lambda}_{400}}[f]$.

to $N_{SQ} = 13402, N_{SQ} = 12696, N_{SQ} = 12967$ solutions of Hi-Fi forward problems for the three choices of f respectively. Figure 4.3(a) shows the sparse grid levels for the activated dimensions at $N = 400$, using the plain SQ algorithm for the approximation of $\mathbb{E}[s]$. The graph indicates that the first two dimensions are the most important, but there isn't a clear decrease in the sparse grid levels utilized for higher dimensions, which is an indication of the complex effect that different dimensions have on the computed QoIs. We also use the mean conductivity $\mathbb{E}[\sigma(\boldsymbol{x}, \boldsymbol{y})] = 3.3\chi_{D_+}(\boldsymbol{x}) + 0.5\exp(0.5)\chi_{D_-}(\boldsymbol{x})$ to compute the value $s(\boldsymbol{E}(\mathbb{E}[\sigma])) = (4.4828 - 5.7186\text{i}) \times 10^{-6}$, which shows in comparison with $\mathbb{E}[s(\boldsymbol{E}(\sigma))]$ in Table 4.2 the effect of non-linearity.

4.2. SQ-EIM-RB algorithm. As a next step, we employ the SQ-EIM-RB algorithm, where now we use the approximation $Q_{\Lambda_N}[\hat{f}]$, with $\hat{f}$ being the EIM-RB representation for $f = s, f = s^2, f = |s|^2$, i.e. $\hat{f} = \hat{z}^s, \hat{f} = \hat{z}^{s^2}, \hat{f} = \hat{z}^{|s|^2}$ respectively. We use a separate simulation for the choices $f = s$ and $f = s^2$ but to save computational effort we compute $Q_{\Lambda_N}[\hat{z}^{s^2}]$ and $Q_{\Lambda_N}[\hat{z}^{|s|^2}]$ using the same simulation, with the profits from the first driving the sparse grid algorithm, and by utilising the same RB space for both quantities as mentioned in section 3.2.3. We additionally set the tolerances as $tol_{\text{EIM-RB}} = 10^2 \cdot tol, tol_{\text{EIM}} = 10^{-2} \cdot tol_{\text{EIM-RB}}, tol_{\text{RB}} = 10^{-1} \cdot tol_{\text{EIM-RB}}$ and we initialize the auxiliary EIM approximation with $N_E = 10$ terms using randomly chosen values for $\boldsymbol{y}$. Choosing an EIM tolerance that is lower than the RB tolerance was necessary in practice to achieve convergence up to the desired accuracy. Figure 4.3(b) shows the convergence of the relative error with respect to the number of indices. We don't have an a priori convergence theory for this case to compare, so our reference is the estimate

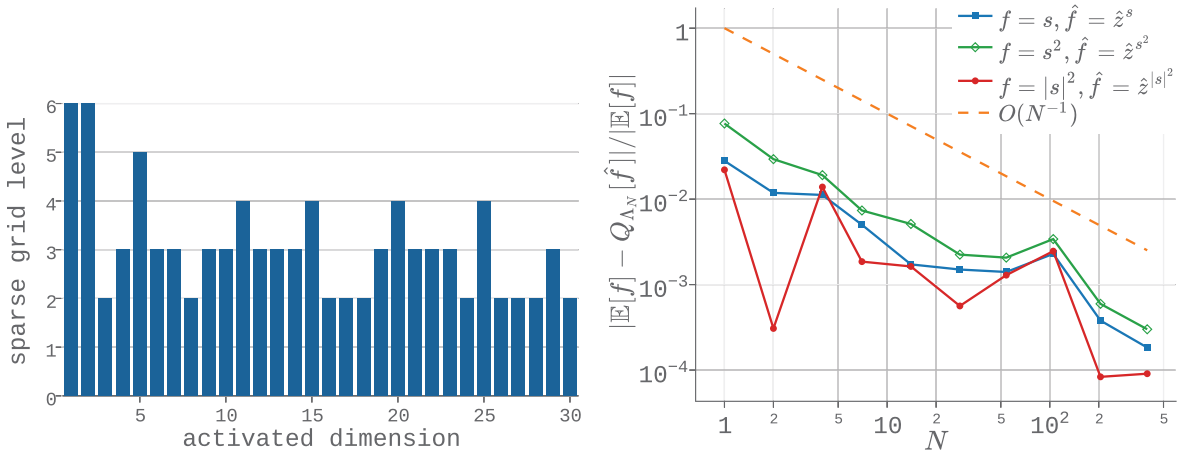

(a) (b)

Figure 4.3: (a) Activated dimensions and corresponding sparse grid levels for the approximation of $\mathbb{E}[s]$ by the plain SQ algorithm. (b) Convergence of relative error $|\mathbb{E}[f] - Q_{\Lambda_N}[\hat{f}]|/|\mathbb{E}[f]|$ with respect to the number of indices N for the SQ-EIM-RB Algorithm 1 with $f = s, f = s^2$ and $f = |s|^2$, and EIM-RB approximations $\hat{f} = \hat{z}^s, \hat{f} = \hat{z}^{s^2}, \hat{f} = \hat{z}^{|s|^2}$ respectively. The "true" value is approximated as $\mathbb{E}[f] \approx Q_{\tilde{\Lambda}_{400}}[f]$.

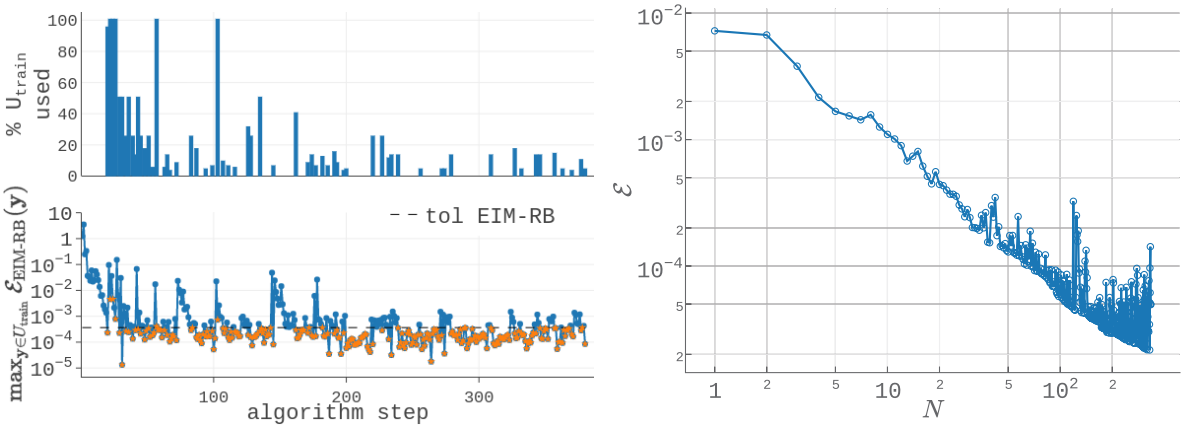

(a) (b)

Figure 4.4: (a) Bottom: behaviour of $\max_{\boldsymbol{y} \in U_{\text{train}}} \mathcal{E}_{\text{EIM-RB}}(\boldsymbol{y})$ as the algorithm runs through the training sets U_{train}. The last considered value of $\max_{\boldsymbol{y} \in U_{\text{train}}} \mathcal{E}_{\text{EIM-RB}}(\boldsymbol{y})$ in each U_{train} is depicted with an orange star. Top: percentage of points in each U_{train} used in the enrichment of the EIM-RB approximation. (b) Sparse grid error indicator $\mathcal{E}$, equal to the profit $P(\boldsymbol{\nu})$ for the chosen index $\boldsymbol{\nu}$, in each iteration of algorithm 1, with respect to the number of indices N.

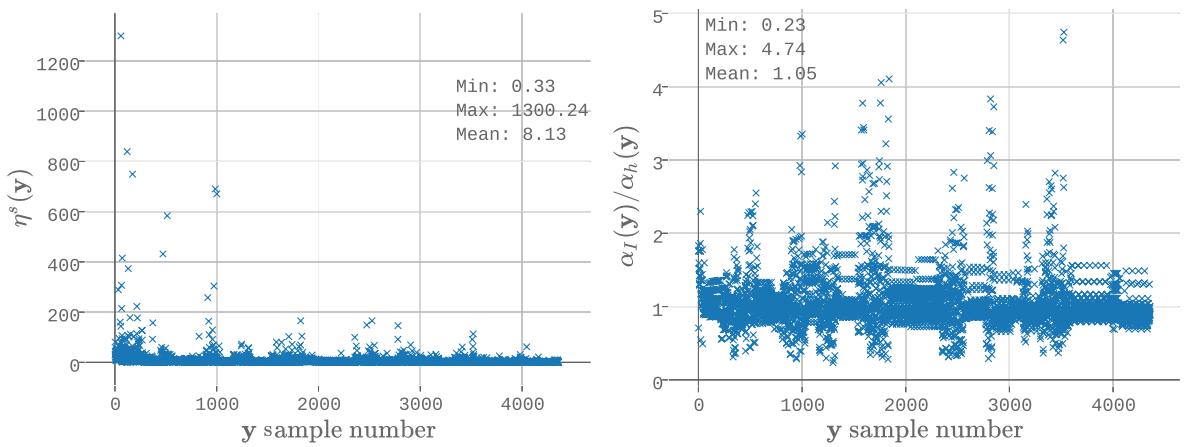

(a) (b)

Figure 4.5: (a) Effectivity $\eta^s(\boldsymbol{y})$ of the error estimator $\Delta^s_{N_I,N_P,N_D}(\boldsymbol{y})$ for each selected $\boldsymbol{y}$. (b) Ratio of interpolated $\alpha_I(\boldsymbol{y})$ to discrete $\alpha_h(\boldsymbol{y})$ coercivity factor for each selected $\boldsymbol{y}$.

	N_I	N_P	$\hat{f}$ evaluations	active dimensions
s	143	86	12530	30
$s^2, \lvert s\rvert^2$	150	69	11279	36

Table 4.1: Number of terms N_I in the EIM approximation, reduced space size $N_P = N_D = N_{D2}$ and number of evaluations of the EIM-RB approximation $\hat{f}$, for the three different choices of f at $N = 400$.

from the SQ theory. The results show an error decay that is comparable to the plain SQ case but with larger fluctuations. Observe that the use of $f = s^2$ to drive the algorithm and build the reduced space affects the performance of the approximation for the case $f = |s|^2$. At $N = 400$, we get the reduced space sizes, number of function evaluations and active dimensions summarized in Table 4.1 and the values outlined in Table 4.2. Figure 4.4(a) shows at the bottom the behaviour of the quantity $\max_{\boldsymbol{y}\in U_{\text{train}}}$ as the algorithm progresses through the training sets U_{train}. We mark the last value of this quantity for each training set (corresponding to the last $\boldsymbol{y}$ in each set or the first $\boldsymbol{y}$ in each set for which the tolerance criterion is satisfied) with an orange star. Therefore an orange star above the tolerance means that all points $\boldsymbol{y}$ in that training set were used for the enrichment of the EIM-RB approximation, while an orange star below the tolerance means that only a percentage of the points were used. This percentage is depicted at the top of Figure 4.4(a). We can also see that there are spikes in the values of $\max_{\boldsymbol{y}\in U_{\text{train}}}$, which can be attributed to training sets that are related with the activation of new dimensions. In Figure 4.4(b), we report the error indicator $\mathcal{E} = P(\boldsymbol{\nu})$ for the chosen indices $\boldsymbol{\nu}$ which shows a clear decrease but with some deterioration as the tolerance limits are approached.

	plain SQ	SQ-EIM-RB
$\mathbb{E}[s]$	$(4.4828 - 5.7186\mathrm{i}) \times 10^{-6}$	$(4.4820 - 5.7218\mathrm{i}) \times 10^{-6}$
$\mathrm{Cov}[s, s]$	$(-1.436 - 0.806\mathrm{i}) \times 10^{-12}$	$(-1.424 - 0.824\mathrm{i}) \times 10^{-12}$
$\mathrm{Cov}[s, \overline{s}]$	1.830×10^{-12}	1.793×10^{-12}

Table 4.2: Values in SI units of the mean $\mathbb{E}[s]$, covariance $\mathrm{Cov}[s, \overline{s}]$ and pseudo-covariance $\mathrm{Cov}[s, s]$ as approximated by the plain SQ (using $Q_{\tilde{\Lambda}_{400}}[f]$) and SQ-EIM-RB (using $Q_{\tilde{\Lambda}_{400}}[\hat{f}]$) methods at $N = 400$.

More information on the EIM-RB approximation scheme can be derived from Figure 4.5(a) which shows the effectivity of the EIM-RB error estimator $\Delta^s_{N_I,N_P,N_D}(\boldsymbol{y})$, defined as $\eta^s(\boldsymbol{y}) = \frac{\Delta^s_{N_I,N_P,N_D}(\boldsymbol{y})}{|s(\boldsymbol{E}_h(\boldsymbol{y})) - \hat{z}^s_{N_I,N_P,N_D}(\boldsymbol{y})|}$. It varies in the range $0.33 - 1300.24$ with a mean equal to 8.13. Values lower than 1 are attributed to the approximation of $\alpha_h(\boldsymbol{y})$ by $\alpha_I(\boldsymbol{y})$, while large values are additionally attributed to the corresponding large condition numbers of the underlying variational problem. Furthermore, Figure 4.5(b) depicts the ratio of the RBF interpolated coercivity factor $\alpha_I(\boldsymbol{y})$ to the discrete coercivity factor $a_h(\boldsymbol{y})$ for each selected $\boldsymbol{y}$. We can see that the ratio varies in the range $0.23 - 4.74$ with a mean that is close to unity, which shows that the RBF interpolant gives a reasonable approximation for most $\boldsymbol{y}$.

5. Conclusion. In this work, we have examined theoretically and numerically a computational framework based on Sparse Grid quadrature and model reduction that enables efficient uncertainty quantification for the low-frequency, time-harmonic Maxwell equations with log-normal conductivity random field and regularized source and receiver representations. We focused on the second-order characterization of the measurement s given by the mean $\mathbb{E}[s]$, the covariance $\mathrm{Cov}[s, \overline{s}]$ and the pseudo-covariance $\mathrm{Cov}[s, s]$. It is shown that the SQ theory applies also for this model, predicting dimension-independent convergence rates that agree with the numerical results produced using a dimension-adaptive algorithm. Additionally, we have described a model reduction scheme based on the weighted Reduced Basis and Empirical Interpolation methods that allows to reduce the computational cost in the case where the dimension of the discretised problem is high. The computational framework we proposed, as outlined in Algorithm 1 is adaptive and it is based on goal-oriented, primal-dual based, a posteriori error estimators. The performance of the combined SQ-EIM-RB algorithm was tested numerically to show the efficiency of the estimators for most sample values and the convergence of the quadrature scheme with rate comparable to the plain SQ case.

Going forward, additional challenges are both theoretical and computational. An a priori convergence estimate for the combined SQ-EIM-RB approach would give more insight into its properties. An additional issue we haven't addressed is the case of many sources and receivers which would be computationally expensive with a straightforward model reduction approach. These topics, together with the application of the framework for the corresponding Bayesian inverse problem, are to be addressed in future work.

Appendix A. Coercivity, continuity and perturbation. We prove here the coercivity and continuity of the sesquilinear form as defined in (2.14), using $\|\cdot\|$ to denote the $L^2(D, \mathbb{C}^3)$

norm.

$$|a(\boldsymbol{u},\boldsymbol{v};\sigma)| \leq |(\mu^{-1}\nabla\times\boldsymbol{u},\nabla\times\boldsymbol{v})| + |\imath\omega|\,|(\sigma\boldsymbol{u},\boldsymbol{v})| \tag{A.1}$$

$$\leq \|\mu^{-1}\|_{L^\infty(D)}\|\nabla\times\boldsymbol{u}\|\|\nabla\times\boldsymbol{v}\| + \omega\|\sigma\|_{L^\infty(D)}\|\boldsymbol{u}\|\|\boldsymbol{v}\| \tag{A.2}$$

$$\leq \max(\mu_{\min}^{-1},\omega\sigma_{\max})(\|\nabla\times\boldsymbol{u}\|\|\nabla\times\boldsymbol{v}\| + \|\boldsymbol{u}\|\|\boldsymbol{v}\|) \tag{A.3}$$

$$\leq \gamma(\|\nabla\times\boldsymbol{u}\|^2 + \|\boldsymbol{u}\|^2)^{1/2}(\|\nabla\times\boldsymbol{v}\|^2 + \|\boldsymbol{v}\|^2)^{1/2} \tag{A.4}$$

$$\leq \gamma\|\boldsymbol{u}\|_{H(\mathrm{curl},D)}\|\boldsymbol{v}\|_{H(\mathrm{curl},D)}, \tag{A.5}$$

with continuity constant $\gamma = \max(\mu_{\min}^{-1},\omega\sigma_{\max})$. It is also coercive on $H(\mathrm{curl},D)$ since for $m\in\mathbb{C}$ with $|m|>0$ we have

$$|m||a(\boldsymbol{u},\boldsymbol{u};\sigma)| \geq |\Re(ma(\boldsymbol{u},\boldsymbol{u};\sigma))| \geq \Re(ma(\boldsymbol{u},\boldsymbol{u};\sigma)) \tag{A.6}$$

$$= \Re(m)\|\nabla\times\boldsymbol{u}\|^2_{\mu^{-1}} + \Im(m)\omega\|\boldsymbol{u}\|^2_{\sigma} \tag{A.7}$$

$$\geq \min\left(\operatorname*{ess\,inf}_{\boldsymbol{x}\in D}(\Re(m)\mu^{-1}), \omega\operatorname*{ess\,inf}_{\boldsymbol{x}\in D}(\Im(m)\sigma)\right)(\|\nabla\times\boldsymbol{u}\|^2 + \|\boldsymbol{u}\|^2) \tag{A.8}$$

$$= \|\boldsymbol{u}\|^2_{H(\mathrm{curl},D)}, \tag{A.9}$$

where we have chosen $\Re(m) = \mu_{\max}$ and $\Im(m) = \frac{1}{\omega\sigma_{\min}}$. The coercivity constant is $\alpha = 1/|m|$.

Suppose for two conductivities σ and $\tilde{\sigma}$ that satisfy the assumption (2.12) we have two solutions of (2.14), $\boldsymbol{E}$ and $\tilde{\boldsymbol{E}}$ respectively (possibly having different coercivity constants $\alpha,\tilde{\alpha}$). Subtracting we get

$$a(\boldsymbol{E},\boldsymbol{v};\sigma) - a(\tilde{\boldsymbol{E}},\boldsymbol{v};\tilde{\sigma}) = 0, \tag{A.10}$$

which gives

$$a(\boldsymbol{E}-\tilde{\boldsymbol{E}},\boldsymbol{v};\sigma) = l(\boldsymbol{v}) = \imath\omega\int_D(\sigma-\tilde{\sigma})\tilde{\boldsymbol{E}}\cdot\overline{\boldsymbol{v}}\,d\boldsymbol{x}. \tag{A.11}$$

Therefore

$$\|\boldsymbol{E}-\tilde{\boldsymbol{E}}\|_V \leq \frac{1}{\alpha}\|l\|_{V^*} \leq \frac{\omega}{\alpha}\|\sigma-\tilde{\sigma}\|_{L^\infty(D)}\|\tilde{\boldsymbol{E}}\|_V \leq \frac{\omega\|f\|_{V^*}}{\min(\alpha,\tilde{\alpha})^2}\|\sigma-\tilde{\sigma}\|_{L^\infty(D)}. \tag{A.12}$$

Appendix B. Properties of anisotropic Whittle-Matérn covariance. The anisotropic Whittle-Matérn covariance can be thought of as the isotropic case under a linear coordinate transformation. Writing $M^{-1} = Q^T\Lambda Q$, where Λ is a diagonal matrix with the eigenvalues of M^{-1} on the diagonal and Q is an orthogonal matrix with the corresponding eigenvectors as columns, we can define new coordinates $\boldsymbol{x}' = \Lambda^{1/2}Q\boldsymbol{x}$, so that $\|\boldsymbol{x}\|_M = \|\boldsymbol{x}'\|_2$. In general, properties of the anisotropic case can be derived from existing analysis using the equivalence of finite-dimensional norms. Moreover, if we define

$$c(r) = \frac{1}{2^{\nu-1}\Gamma(\nu)}\,(r)^\nu\,K_\nu\,(r)\,, \tag{B.1}$$

then the Fourier transform of $C(\boldsymbol{x},\boldsymbol{y}) = c(\|\boldsymbol{x}-\boldsymbol{y}\|_2)$ in d spatial dimensions is

$$f(\boldsymbol{w}) = \frac{\Gamma(\nu+d/2)}{\Gamma(\nu)}\frac{2^{d/2}}{(1+\|\boldsymbol{w}\|_2^2)^{\nu+d/2}}, \tag{B.2}$$

and the Fourier transform of $C_A = C(\boldsymbol{x'},\boldsymbol{y'}) = c(\|\boldsymbol{x'}-\boldsymbol{y'}\|_2) = c(\|\boldsymbol{x}-\boldsymbol{y}\|_M)$ is $g(\boldsymbol{w}) = \sqrt{\det M} f(\sqrt{\boldsymbol{w}^T M \boldsymbol{w}})$. Using a theorem from Widom [69], one can show that

$$\lambda_j \le K(D,M,d,\nu) j^{-(2\nu/d+1)}. \tag{B.3}$$

An alternative way to derive this bound is to notice that $C(\boldsymbol{x'},\boldsymbol{y'})$ obeys the conditions in [7]

$$k(1+\|\boldsymbol{w}\|_2^2)^{-(\nu+d/2)} \le g(\boldsymbol{w}) \le K(1+\|\boldsymbol{w}\|_2^2)^{-(\nu+d/2)}, \quad 0<k\le K. \tag{B.4}$$

and

$$\lim_{R\to\infty}\int_{\|\boldsymbol{x'}\|>R} |\partial^{\boldsymbol{\alpha}} c(\boldsymbol{x'})|\, d\boldsymbol{x'} = 0, \quad |\boldsymbol{\alpha}| \le 2\lceil \nu + d/2\rceil. \tag{B.5}$$

Additionally, in [7] it is proved that these conditions lead to the following bound for the eigenfunctions

$$\|\phi_j\|_{L^\infty(D)} \le K\lambda_j^{-s/(2\nu+d)}, \quad d/2 < s < \nu + d/2, \tag{B.6}$$

which taking $s = d/2+\epsilon$, with $\epsilon>0$ sufficiently small, and using (B.3) gives the (not always sharp) bound

$$\|\psi_j\|_{L^\infty(D)} \le K j^{-\nu/d+\epsilon}. \tag{B.7}$$

Appendix C. Parametric partial derivatives and weighted Sobolev-type norms. We start by finding an expression for the partial derivative $\partial^{\boldsymbol{\mu}}\boldsymbol{E}(\boldsymbol{y})$ for $\boldsymbol{\mu} = \boldsymbol{e}_j = (\delta_{ij})_{i\ge1}$, $j\in\mathbb{N}$ as in [6, 28]. We consider two solutions $\boldsymbol{E}(\boldsymbol{y}+h\boldsymbol{e}_j)$ and $\boldsymbol{E}(\boldsymbol{y})$ to problem (2.36) with $|h|<1$, for the same source term and the same $\sigma_*,\sigma_0,\sigma_+$ and define the function

$$\boldsymbol{w}_h(\boldsymbol{y}) = \frac{\boldsymbol{E}(\boldsymbol{y}+h\boldsymbol{e}_j)-\boldsymbol{E}(\boldsymbol{y})}{h}. \tag{C.1}$$

so that $\lim_{h\to0}\boldsymbol{w}_h = \partial^{\boldsymbol{\mu}}\boldsymbol{E}$. Subtracting the two variational formulations we get

$$a(\boldsymbol{E}(\boldsymbol{y}+h\boldsymbol{e}_j),\boldsymbol{v};\sigma(\boldsymbol{y}+h\boldsymbol{e}_j)) - a(\boldsymbol{E}(\boldsymbol{y}),\boldsymbol{v};\sigma(\boldsymbol{y})) = 0, \tag{C.2}$$

which leads to

$$a(\boldsymbol{w}_h(\boldsymbol{y}),v;\sigma(\boldsymbol{y})) = \imath\omega\int_D \frac{\sigma(\boldsymbol{y}+h\boldsymbol{e}_j)-\sigma(\boldsymbol{y})}{h}\boldsymbol{E}(\boldsymbol{y}+h\boldsymbol{e}_j)\cdot\overline{\boldsymbol{v}}\, d\boldsymbol{x} = l_h(\boldsymbol{v}). \tag{C.3}$$

If $l_0(\boldsymbol{v}) = \imath\omega(\partial^{\boldsymbol{\mu}}\sigma(\boldsymbol{y})\boldsymbol{E}(\boldsymbol{y}), \boldsymbol{v})_{L^2(D,\mathbb{C}^3)}$, then using (A.12) we have

(C.4)
$$|l_h(\boldsymbol{v}) - l_0(\boldsymbol{v})| = \omega \left| \int_D \left(\frac{\sigma(\boldsymbol{y}+h\boldsymbol{e}_j)-\sigma(\boldsymbol{y})}{h} \boldsymbol{E}(\boldsymbol{y}+h\boldsymbol{e}_j) - \partial^{\boldsymbol{\mu}}\sigma(\boldsymbol{y})\boldsymbol{E}(\boldsymbol{y}) \right) \cdot \overline{\boldsymbol{v}}\, d\boldsymbol{x} \right|$$

(C.5)
$$\leq K\omega \left(\left\| \frac{\sigma(\boldsymbol{y}+h\boldsymbol{e}_j)-\sigma(\boldsymbol{y})}{h} \right\|_{L^\infty(D)} \|\boldsymbol{E}(\boldsymbol{y}+h\boldsymbol{e}_j) - \boldsymbol{E}(\boldsymbol{y})\|_V \right.$$

(C.6)
$$\left. + \left\| \frac{\sigma(\boldsymbol{y}+h\boldsymbol{e}_j)-\sigma(\boldsymbol{y})}{h} - \partial^{\boldsymbol{\mu}}\sigma(\boldsymbol{y}) \right\|_{L^\infty(D)} \|\boldsymbol{E}(\boldsymbol{y})\|_V \right) \|\boldsymbol{v}\|_V$$

(C.7)
$$\leq K\omega \left(\frac{\omega\|f\|_{V^*}}{\min(\alpha(\boldsymbol{y}), \alpha(\boldsymbol{y}+h\boldsymbol{e}_j))^2} \left\| \frac{\sigma(\boldsymbol{y}+h\boldsymbol{e}_j)-\sigma(\boldsymbol{y})}{h} \right\|_{L^\infty(D)} \|\sigma(\boldsymbol{y}+h\boldsymbol{e}_j) - \sigma(\boldsymbol{y})\|_{L^\infty(D)} \right.$$

(C.8)
$$\left. + \left\| \frac{\sigma(\boldsymbol{y}+h\boldsymbol{e}_j)-\sigma(\boldsymbol{y})}{h} - \partial^{\boldsymbol{\mu}}\sigma(\boldsymbol{y}) \right\|_{L^\infty(D)} \frac{\|f\|_{V^*}}{\alpha(\boldsymbol{y})} \right) \|\boldsymbol{v}\|_V \to 0 \quad \text{as} \quad h \to 0$$

which shows that, under our assumptions on σ, $l_h \to l_0$ in V^* as $h \to 0$. So the partial derivative $\partial^{\boldsymbol{\mu}}\boldsymbol{E}(\boldsymbol{y}) \in V$ is the solution to

$$a(\partial^{\boldsymbol{\mu}}\boldsymbol{E}(\boldsymbol{y}), \boldsymbol{v}; \sigma(\boldsymbol{y})) = \imath\omega \int_D \partial^{\boldsymbol{\mu}}\sigma(\boldsymbol{y})\boldsymbol{E}(\boldsymbol{y}) \cdot \overline{\boldsymbol{v}}\, d\boldsymbol{x}, \quad \boldsymbol{\mu} = \boldsymbol{e}_j,\ \forall \boldsymbol{v} \in V, \tag{C.9}$$

and by recursion it follows that

$$a(\partial^{\boldsymbol{\mu}}\boldsymbol{E}(\boldsymbol{y}), \boldsymbol{v}; \sigma(\boldsymbol{y})) = \imath\omega \sum_{\substack{\boldsymbol{\nu} \leq \boldsymbol{\mu} \\ \boldsymbol{\nu} \neq \boldsymbol{\mu}}} \binom{\boldsymbol{\mu}}{\boldsymbol{\nu}} \int_D \partial^{\boldsymbol{\mu}-\boldsymbol{\nu}}\sigma(\boldsymbol{y})\partial^{\boldsymbol{\nu}}\boldsymbol{E}(\boldsymbol{y}) \cdot \overline{\boldsymbol{v}}\, d\boldsymbol{x}, \quad \boldsymbol{\mu}, \boldsymbol{\nu} \in \mathcal{F}, \tag{C.10}$$

The partial derivatives of the parameter are given by

$$\partial^{\boldsymbol{\mu}-\boldsymbol{\nu}}\sigma(\boldsymbol{y}) = \chi_{D_-}(\sigma(\boldsymbol{y}) - \sigma_*)\boldsymbol{\psi}^{\boldsymbol{\mu}-\boldsymbol{\nu}}, \quad \boldsymbol{\psi}^{\boldsymbol{\mu}-\boldsymbol{\nu}} = \prod_{j \geq 1} \psi_j^{\mu_j - \nu_j} \tag{C.11}$$

which leads to the bound (see e.g. [40])

$$\left\| \frac{\partial^{\boldsymbol{\mu}-\boldsymbol{\nu}}\sigma(\boldsymbol{y})}{\sigma(\boldsymbol{y})} \right\|_{L^\infty(D)} \leq \|\boldsymbol{\psi}\|_{L^\infty(D)}^{\boldsymbol{\mu}-\boldsymbol{\nu}}. \tag{C.12}$$

Recalling the continuity and coercivity of the sesquilinear form gives

$$\alpha(\boldsymbol{y})\|\boldsymbol{u}(\boldsymbol{y})\|_V^2 \leq |a(\boldsymbol{u}(\boldsymbol{y}), \boldsymbol{u}(\boldsymbol{y}); \sigma(\boldsymbol{y}))| \leq \gamma(\boldsymbol{y})\|\boldsymbol{u}(\boldsymbol{y})\|_V^2. \tag{C.13}$$

We define an equivalent L^2 norm for any strictly positive function z by

$$\|\boldsymbol{u}\|^2_{L^2(D,\mathbb{C}^3,z)} = \int_D z\boldsymbol{u}\cdot\overline{\boldsymbol{u}}\,d\boldsymbol{x} = \|\sqrt{z}\boldsymbol{u}\|^2_{L^2(D,\mathbb{C}^3)}. \tag{C.14}$$

Notice that

$$\|\boldsymbol{u}(\boldsymbol{y})\|_{L^2(D,\mathbb{C}^3,\sigma(\boldsymbol{y}))} \le \frac{1}{\sqrt{\omega}}\,|a(\boldsymbol{u}(\boldsymbol{y}),\boldsymbol{u}(\boldsymbol{y});\sigma(\boldsymbol{y}))|^{1/2} \le \sqrt{\frac{\gamma(\boldsymbol{y})}{\omega}}\|\boldsymbol{u}(\boldsymbol{y})\|_V. \tag{C.15}$$

We use (C.13), (C.15), (C.10), (C.12) and the Cauchy-Schwarz inequality to get (analogously to relation 77 in [6])

(C.16)

$$\|\partial^{\boldsymbol{\mu}}\boldsymbol{E}(\boldsymbol{y})\|_V^2 \le \frac{1}{\alpha(\boldsymbol{y})}|a(\partial^{\boldsymbol{\mu}}\boldsymbol{E}(\boldsymbol{y}),\partial^{\boldsymbol{\mu}}\boldsymbol{E}(\boldsymbol{y});\sigma(\boldsymbol{y}))|$$

$$\le \frac{\omega}{\alpha(\boldsymbol{y})}\left|\sum_{\substack{\boldsymbol{\nu}\le\boldsymbol{\mu}\\ \boldsymbol{\nu}\neq\boldsymbol{\mu}}}\binom{\boldsymbol{\mu}}{\boldsymbol{\nu}}\int_D \partial^{\boldsymbol{\mu}-\boldsymbol{\nu}}\sigma(\boldsymbol{y})\partial^{\boldsymbol{\nu}}\boldsymbol{E}(\boldsymbol{y})\cdot\overline{\partial^{\boldsymbol{\mu}}\boldsymbol{E}(\boldsymbol{y})}\,d\boldsymbol{x}\right| \tag{C.17}$$

$$\le \frac{\omega}{\alpha(\boldsymbol{y})}\sum_{\substack{\boldsymbol{\nu}\le\boldsymbol{\mu}\\ \boldsymbol{\nu}\neq\boldsymbol{\mu}}}\binom{\boldsymbol{\mu}}{\boldsymbol{\nu}}\left\|\frac{\partial^{\boldsymbol{\mu}-\boldsymbol{\nu}}\sigma(\boldsymbol{y})}{\sigma(\boldsymbol{y})}\right\|_{L^\infty(D)}\left|\int_D \sqrt{\sigma(\boldsymbol{y})}\sqrt{\sigma(\boldsymbol{y})}\partial^{\boldsymbol{\nu}}\boldsymbol{E}(\boldsymbol{y})\cdot\overline{\partial^{\boldsymbol{\mu}}\boldsymbol{E}(\boldsymbol{y})}\,d\boldsymbol{x}\right| \tag{C.18}$$

$$\le \frac{\omega}{\alpha(\boldsymbol{y})}\sum_{\substack{\boldsymbol{\nu}\le\boldsymbol{\mu}\\ \boldsymbol{\nu}\neq\boldsymbol{\mu}}}\binom{\boldsymbol{\mu}}{\boldsymbol{\nu}}\|\boldsymbol{\psi}\|^{\boldsymbol{\mu}-\boldsymbol{\nu}}_{L^\infty(D)}\|\partial^{\boldsymbol{\nu}}\boldsymbol{E}(\boldsymbol{y})\|_{L^2(D,\mathbb{C}^3,\sigma)}\|\partial^{\boldsymbol{\mu}}\boldsymbol{E}(\boldsymbol{y})\|_{L^2(D,\mathbb{C}^3,\sigma)} \tag{C.19}$$

$$\le K_{\boldsymbol{\mu}}\frac{\gamma(\boldsymbol{y})}{\alpha(\boldsymbol{y})}\|\partial^{\boldsymbol{\mu}}\boldsymbol{E}(\boldsymbol{y})\|_V\sum_{\substack{\boldsymbol{\nu}\le\boldsymbol{\mu}\\ \boldsymbol{\nu}\neq\boldsymbol{\mu}}}\|\partial^{\boldsymbol{\nu}}\boldsymbol{E}(\boldsymbol{y})\|_V, \tag{C.20}$$

with constant $K_{\boldsymbol{\mu}} = \max_{\substack{\boldsymbol{\nu}\le\boldsymbol{\mu}\\ \boldsymbol{\nu}\neq\boldsymbol{\mu}}}\|\boldsymbol{\psi}\|^{\boldsymbol{\mu}-\boldsymbol{\nu}}_{L^\infty(D)}\binom{|\boldsymbol{\mu}|}{\lfloor|\boldsymbol{\mu}|/2\rfloor}^{\#(\mathrm{supp}(\boldsymbol{\mu}))} > 0$, where $\lfloor\cdot\rfloor$ denotes the floor function. We can apply this relation recursively to arrive at

$$\|\partial^{\boldsymbol{\mu}}\boldsymbol{E}(\boldsymbol{y})\|_V \le K\left(\frac{\gamma(\boldsymbol{y})}{\alpha(\boldsymbol{y})}\right)^{|\boldsymbol{\mu}|}\frac{\|f\|_{V^*}}{\alpha(\boldsymbol{y})}, \quad \boldsymbol{\mu}\in\mathcal{F}, \tag{C.21}$$

which according to our assumptions on σ, guarantees the finiteness of $\|\partial^{\boldsymbol{\mu}}\boldsymbol{E}(\boldsymbol{y})\|_{L^p(U,V)}$ for $0\le p<\infty$.

Now we prove that an analogue to Theorem 4.1 in [6] applies. For an integer $r\ge 1$ and a sequence $(\rho_j)_{j\ge1}$ such that

$$\sup_{\boldsymbol{x}\in D_-}\sum_{j=1}^{\infty}\rho_j|\psi_j(\boldsymbol{x})| = K < C(r) = \frac{\ln 2}{\sqrt{r}}, \tag{C.22}$$

there exists a constant $C(K,r)$ such that

$$\sum_{\|\boldsymbol{\mu}\|_{l^\infty}\leq r} \frac{\boldsymbol{\rho}^{2\boldsymbol{\mu}}}{\boldsymbol{\mu}!}|a(\partial^{\boldsymbol{\mu}}\boldsymbol{E}(\boldsymbol{y}),\partial^{\boldsymbol{\mu}}\boldsymbol{E}(\boldsymbol{y});\sigma(\boldsymbol{y}))| \leq C(K,r)|a(\boldsymbol{E}(\boldsymbol{y}),\boldsymbol{E}(\boldsymbol{y});\sigma(\boldsymbol{y}))|. \tag{C.23}$$

The proof follows [6]; we describe here only the required changes. For $k \geq 0$ and

$$\eta_k = \sum_{\substack{|\boldsymbol{\mu}|=k \\ \|\boldsymbol{\mu}\|_{l^\infty}\leq r}} \frac{\boldsymbol{\rho}^{2\boldsymbol{\mu}}}{\boldsymbol{\mu}!}|a(\partial^{\boldsymbol{\mu}}\boldsymbol{E}(\boldsymbol{y}),\partial^{\boldsymbol{\mu}}\boldsymbol{E}(\boldsymbol{y});\sigma(\boldsymbol{y}))|, \tag{C.24}$$

it is only required to prove that $\eta_k \leq \eta_0\delta^k$ for a fixed $\delta < 1$. Using the notation

$$\epsilon(\boldsymbol{\mu},\boldsymbol{\nu}) = \frac{\sqrt{\boldsymbol{\mu}!}\boldsymbol{\rho}^{\boldsymbol{\mu}-\boldsymbol{\nu}}|\boldsymbol{\psi}|^{\boldsymbol{\mu}-\boldsymbol{\nu}}}{\sqrt{\boldsymbol{\nu}!}(\boldsymbol{\mu}-\boldsymbol{\nu})!}, \tag{C.25}$$

we have from (C.10) and the Cauchy-Schwarz inequality that

$$\frac{\eta_k}{\omega} \leq \int_D \sum_{\substack{|\boldsymbol{\mu}|=k \\ \|\boldsymbol{\mu}\|_{l^\infty}\leq r}} \left(\sum_{\substack{\boldsymbol{\nu}\leq\boldsymbol{\mu} \\ \boldsymbol{\nu}\neq\boldsymbol{\mu}}} \epsilon(\boldsymbol{\mu},\boldsymbol{\nu})\sigma(\boldsymbol{y})\frac{|\boldsymbol{\rho}^{\boldsymbol{\nu}}\partial^{\boldsymbol{\nu}}\boldsymbol{E}(\boldsymbol{y})|^2}{\boldsymbol{\nu}!}\right)^{\frac{1}{2}} \left(\sum_{\substack{\boldsymbol{\nu}\leq\boldsymbol{\mu} \\ \boldsymbol{\nu}\neq\boldsymbol{\mu}}} \epsilon(\boldsymbol{\mu},\boldsymbol{\nu})\sigma(\boldsymbol{y})\frac{|\boldsymbol{\rho}^{\boldsymbol{\mu}}\partial^{\boldsymbol{\mu}}\boldsymbol{E}(\boldsymbol{y})|^2}{\boldsymbol{\mu}!}\right)^{\frac{1}{2}} d\boldsymbol{x}. \tag{C.26}$$

Defining also

$$\tau_k = \sum_{\substack{|\boldsymbol{\mu}|=k \\ \|\boldsymbol{\mu}\|_{l^\infty}\leq r}} \frac{\boldsymbol{\rho}^{2\boldsymbol{\mu}}}{\boldsymbol{\mu}!}\|\partial^{\boldsymbol{\mu}}\boldsymbol{E}(\boldsymbol{y})\|^2_{L^2(D,\mathbb{C}^3,\sigma)}, \tag{C.27}$$

and following the steps in [6] leads to

$$\frac{\eta_k}{\omega} \leq \left(\sum_{l=0}^{k-1}\frac{(\sqrt{r}K)^{k-l}}{(k-l)!}\tau_l\right)^{1/2}\tau_k^{1/2}. \tag{C.28}$$

Noticing that $\tau_k \leq \frac{\eta_k}{\omega}$ and following the last argument in [6] completes the proof.

Finally, we prove that Assumption 3.3 applies, i.e. given $0 < p < 1$, $q = 2p/(2-p)$, $r > 10/q$ and a positive sequence $\boldsymbol{\rho} = (\rho_j)_{j\geq 1}$ such that $(\rho_j^{-1})_{j\geq 1} \in l^q(\mathbb{N})$, there holds

$$\sum_{\|\boldsymbol{\mu}\|_{l^\infty}\leq r} \frac{\boldsymbol{\rho}^{2\boldsymbol{\mu}}}{\boldsymbol{\mu}!}\int_U \|\partial^{\boldsymbol{\mu}}\boldsymbol{E}(\boldsymbol{y})\|_V^2\, d\gamma_G(\boldsymbol{y}) < \infty. \tag{C.29}$$

Assuming an integer $r \geq 1$ and a positive sequence $(\rho_j)_{j\geq 1}$ such that (C.22) holds, we start

from (C.13), integrate over U and sum over $\|\boldsymbol{\mu}\|_{l^\infty} \le r$ to obtain

$$\sum_{\|\boldsymbol{\mu}\|_{l^\infty}\le r} \frac{\boldsymbol{\rho}^{2\boldsymbol{\mu}}}{\boldsymbol{\mu}!} \int_U \|\partial^{\boldsymbol{\mu}} \boldsymbol{E}(\boldsymbol{y})\|_V^2 \, d\gamma_G(\boldsymbol{y}) \tag{C.30}$$

$$\le \int_D \frac{1}{\alpha(\boldsymbol{y})} \left(\sum_{\|\boldsymbol{\mu}\|_{l^\infty}\le r} \frac{\boldsymbol{\rho}^{2\boldsymbol{\mu}}}{\boldsymbol{\mu}!} |a(\partial^{\boldsymbol{\mu}} \boldsymbol{E}(\boldsymbol{y}), \partial^{\boldsymbol{\mu}} \boldsymbol{E}(\boldsymbol{y}); \sigma(\boldsymbol{y}))| \right) d\gamma_G(\boldsymbol{y}) \tag{C.31}$$

$$\le C(K,r) \int_U \frac{1}{\alpha(\boldsymbol{y})} |a(\boldsymbol{E}(\boldsymbol{y}), \boldsymbol{E}(\boldsymbol{y}); \sigma(\boldsymbol{y}))| \, d\gamma_G(\boldsymbol{y}) \tag{C.32}$$

$$\le C(K,r) \int_U \frac{\gamma(\boldsymbol{y})}{\alpha(\boldsymbol{y})} \|\boldsymbol{E}(\boldsymbol{y})\|_V^2 \, d\gamma_G(\boldsymbol{y}) \tag{C.33}$$

$$\le C(K,r) \|f\|_{V^*}^2 \int_U \frac{\gamma(\boldsymbol{y})}{\alpha(\boldsymbol{y})^3} \, d\gamma_G(\boldsymbol{y}) < \infty, \tag{C.34}$$

where the last term is finite due to our assumptions on $\sigma(\boldsymbol{x}, \boldsymbol{y})$.

Since we assumed $r \ge 1$, we can choose r to be smallest integer such that $r > 10/q$. Then the assumption $\sup_{\boldsymbol{x}\in D_-} \sum_{j=1}^\infty \rho_j |\psi_j(\boldsymbol{x})| < \infty$ means up to multiplication with a constant that (C.22) holds and thus (C.29) follows, proving the theorem.

Appendix D. A posteriori error estimate derivation. For $z = s$ we have (omitting $\boldsymbol{y}$-dependence)

$$\begin{aligned}
&|z(\boldsymbol{E}_h) - \hat{z}_{N_I,N_P,N_D}| = |z(\boldsymbol{E}_h) - z(\boldsymbol{E}_{N_I,N_P}) + f(\boldsymbol{E}^{\mathrm{du}}_{N_I,N_D}) - a_{N_I}(\boldsymbol{E}_{N_I,N_P}, \boldsymbol{E}^{\mathrm{du}}_{N_I,N_D})| \\
&= |s(\boldsymbol{\varepsilon}_{N_I,N_P}) + a(\boldsymbol{E}_h, \boldsymbol{E}^{\mathrm{du}}_{N_I,N_D}) - a_{N_I}(\boldsymbol{E}_{N_I,N_P}, \boldsymbol{E}^{\mathrm{du}}_{N_I,N_D})| \\
&= | - a_{N_I}(\boldsymbol{\varepsilon}_{N_I,N_P}, \boldsymbol{E}^{\mathrm{du}}_{h,N_I}) + a(\boldsymbol{E}_h, \boldsymbol{E}^{\mathrm{du}}_{N_I,N_D}) \\
&\quad + a_{N_I}(\boldsymbol{\varepsilon}_{N_I,N_P}, \boldsymbol{E}^{\mathrm{du}}_{N_I,N_D}) - a_{N_I}(\boldsymbol{E}_h, \boldsymbol{E}^{\mathrm{du}}_{N_I,N_D})| \\
&= | - a_{N_I}(\boldsymbol{\varepsilon}_{N_I,N_P}, \boldsymbol{\varepsilon}^{\mathrm{du}}_{N_D}) + a(\boldsymbol{E}_{N_I,N_P} + \boldsymbol{\varepsilon}_{N_I,N_P}, \boldsymbol{E}^{\mathrm{du}}_{N_I,N_D}) \\
&\quad - a_{N_I}(\boldsymbol{E}_{N_I,N_P} + \boldsymbol{\varepsilon}_{N_I,N_P}, \boldsymbol{E}^{\mathrm{du}}_{N_I,N_D})| \\
&= | - r^{\mathrm{du}}_{N_I,N_D}(\boldsymbol{\varepsilon}_{N_I,N_P}; \boldsymbol{y}) + a(\boldsymbol{E}_{N_I,N_P}, \boldsymbol{E}^{\mathrm{du}}_{N_I,N_D}) - a_{N_I}(\boldsymbol{E}_{N_I,N_P}, \boldsymbol{E}^{\mathrm{du}}_{N_I,N_D}) \\
&\quad + a(\boldsymbol{\varepsilon}_{N_I,N_P}, \boldsymbol{E}^{\mathrm{du}}_{N_I,N_D}) - a_{N_I}(\boldsymbol{\varepsilon}_{N_I,N_P}, \boldsymbol{E}^{\mathrm{du}}_{N_I,N_D})| \\
&\lessapprox \|r^{\mathrm{du}}_{N_I,N_D}\|_{V_h^*} \|\boldsymbol{\varepsilon}_{N_I,N_P}\|_V + \delta^a_{N_I,N_E}(\boldsymbol{E}_{N_I,N_P}, \boldsymbol{E}^{\mathrm{du}}_{N_I,N_D}; \boldsymbol{y}) \\
&\quad + \|\boldsymbol{\varepsilon}_{N_I,N_P}\|_V \|\delta^a_{N_I,N_E}(\cdot, \boldsymbol{E}^{\mathrm{du}}_{N_I,N_D}; \boldsymbol{y})\|_{V_h^*} \\
&\lessapprox \frac{\left(\|r^{\mathrm{du}}_{N_I,N_D}\|_{V_h^*} + \|\delta^a_{N_I,N_E}(\cdot, \boldsymbol{E}^{\mathrm{du}}_{N_I,N_D}; \boldsymbol{y})\|_{V_h^*}\right) \left(\|r^{\mathrm{pr}}_{N_I,N_P}\|_{V_h^*} + \|\delta^a_{N_I,N_E}(\boldsymbol{E}_{N_I,N_P}, \cdot; \boldsymbol{y})\|_{V_h^*}\right)}{\alpha_h} \\
&\quad + \delta^a_{N_I,N_E}(\boldsymbol{E}_{N_I,N_P}, \boldsymbol{E}^{\mathrm{du}}_{N_I,N_D}; \boldsymbol{y}) := \Delta^z_{N_I,N_P,N_D}.
\end{aligned}$$

REFERENCES

[1] R. J. Adler and J. E. Taylor, *Random fields and geometry*, vol. 115, Springer Science & Business Media, 2009, https://doi.org/10.1007/978-0-387-48116-6.

[2] G. S. Alberti, *Hölder regularity for maxwell's equations under minimal assumptions on the coefficients*, Calculus of Variations and Partial Differential Equations, 57 (2018), https://doi.org/10.1007/s00526-018-1358-2.

[3] P. R. Amestoy, I. S. Duff, J.-Y. L'Excellent, and J. Koster, *A fully asynchronous multifrontal solver using distributed dynamic scheduling*, SIAM Journal on Matrix Analysis and Applications, 23 (2001), pp. 15–41, https://doi.org/10.1137/s0895479899358194.

[4] I. Babuška, F. Nobile, and R. Tempone, *A stochastic collocation method for elliptic partial differential equations with random input data*, SIAM Journal on Numerical Analysis, 45 (2007), pp. 1005–1034, https://doi.org/10.1137/050645142.

[5] I. Babuška, R. Tempone, and G. E. Zouraris, *Galerkin finite element approximations of stochastic elliptic partial differential equations*, SIAM Journal on Numerical Analysis, 42 (2004), pp. 800–825, https://doi.org/10.1137/s0036142902418680.

[6] M. Bachmayr, A. Cohen, R. DeVore, and G. Migliorati, *Sparse polynomial approximation of parametric elliptic PDEs. part II: lognormal coefficients*, ESAIM: Mathematical Modelling and Numerical Analysis, 51 (2016), pp. 341–363, https://doi.org/10.1051/m2an/2016051.

[7] M. Bachmayr, A. Cohen, and G. Migliorati, *Representations of gaussian random fields and approximation of elliptic pdes with lognormal coefficients*, Journal of Fourier Analysis and Applications, (2017), https://doi.org/10.1007/s00041-017-9539-5.

[8] J. Bäck, F. Nobile, L. Tamellini, and R. Tempone, *Stochastic spectral galerkin and collocation methods for pdes with random coefficients: A numerical comparison*, in Lecture Notes in Computational Science and Engineering, J. S. Hesthaven and E. M. Rønquist, eds., Springer Berlin Heidelberg, Berlin, Heidelberg, sep 2011, pp. 43–62, https://doi.org/10.1007/978-3-642-15337-2_3.

[9] M. Barrault, Y. Maday, N. C. Nguyen, and A. T. Patera, *An 'empirical interpolation' method: application to efficient reduced-basis discretization of partial differential equations*, Comptes Rendus Mathematique, 339 (2004), pp. 667–672, https://doi.org/10.1016/j.crma.2004.08.006.

[10] P. Benner and M. Hess, *Reduced basis approximations for maxwell's equations in dispersive media*, in Model Reduction of Parametrized Systems, P. Benner, M. Ohlberger, A. Patera, G. Rozza, and K. Urban, eds., Springer International Publishing, Cham, 2017, pp. 107–119, https://doi.org/10.1007/978-3-319-58786-8_7.

[11] *Model Reduction and Approximation: Theory and Algorithms (Computational Science & Engineering)*, SIAM, July 2017, https://doi.org/10.1137/1.9781611974829.

[12] P. Benner and J. Schneider, *Uncertainty quantification for maxwell's equations using stochastic collocation and model order reduction*, International Journal for Uncertainty Quantification, 5 (2015), pp. 195–208, https://doi.org/10.1615/int.j.uncertaintyquantification.2015010170.

[13] P. Binev, A. Cohen, W. Dahmen, R. DeVore, G. Petrova, and P. Wojtaszczyk, *Convergence rates for greedy algorithms in reduced basis methods*, SIAM Journal on Mathematical Analysis, 43 (2011), pp. 1457–1472, https://doi.org/10.1137/100795772.

[14] H.-J. Bungartz and M. Griebel, *Sparse grids*, Acta Numerica, 13 (2004), pp. 147–269, https://doi.org/10.1017/S0962492904000182.

[15] J. Charrier, *Strong and weak error estimates for elliptic partial differential equations with random coefficients*, SIAM Journal on Numerical Analysis, 50 (2012), pp. 216–246, https://doi.org/10.1137/100800531.

[16] J. Charrier and A. Debussche, *Weak truncation error estimates for elliptic pdes with lognormal coefficients*, Stochastic Partial Differential Equations: Analysis and Computations, 1 (2013), pp. 63–93, https://doi.org/10.1007/s40072-013-0006-2.

[17] P. Chen, *Sparse quadrature for high-dimensional integration with gaussian measure*, ESAIM: M2AN, 52 (2018), pp. 631–657, https://doi.org/10.1051/m2an/2018012.

[18] P. Chen and A. Quarteroni, *A new algorithm for high-dimensional uncertainty quantification based on dimension-adaptive sparse grid approximation and reduced basis methods*, Journal of Computational Physics, 298 (2015), pp. 176–193, https://doi.org/10.1016/j.jcp.2015.06.006.

[19] P. Chen, A. Quarteroni, and G. Rozza, *A weighted reduced basis method for elliptic partial differential equations with random input data*, SIAM Journal on Numerical Analysis, 51 (2013), pp. 3163–3185, https://doi.org/10.1137/130905253.

[20] P. Chen, A. Quarteroni, and G. Rozza, *A weighted empirical interpolation method: a priori convergence analysis and applications*, ESAIM: M2AN, 48 (2014), pp. 943–953, https://doi.org/10.1051/m2an/2013128.

[21] P. Chen and C. Schwab, *Sparse-grid, reduced-basis bayesian inversion*, Computer Methods in Applied Mechanics and Engineering, 297 (2015), pp. 84–115, https://doi.org/10.1016/j.cma.2015.08.006.

[22] P. Chen and C. Schwab, *Sparse-grid, reduced-basis bayesian inversion: Nonaffine-parametric nonlinear equations*, Journal of Computational Physics, 316 (2016), pp. 470–503, https://doi.org/10.1016/j.jcp.2016.02.055.

[23] Y. Chen, J. S. Hesthaven, Y. Maday, and J. Rodríguez, *Certified reduced basis methods and output bounds for the harmonic maxwell's equations*, SIAM Journal on Scientific Computing, 32 (2010), pp. 970–996, https://doi.org/10.1137/09075250X.

[24] A. Chkifa, A. Cohen, and C. Schwab, *High-dimensional adaptive sparse polynomial interpolation and applications to parametric pdes*, Foundations of Computational Mathematics, 14 (2014), pp. 601–633, https://doi.org/10.1007/s10208-013-9154-z.

[25] A. Chkifa, A. Cohen, and C. Schwab, *Breaking the curse of dimensionality in sparse polynomial approximation of parametric PDEs*, Journal de Mathématiques Pures et Appliqués, 103 (2015), pp. 400–428, https://doi.org/10.1016/j.matpur.2014.04.009.

[26] A. Cohen, M. Bachmayr, and G. Migliorati, *Sparse polynomial approximation of parametric elliptic PDEs. part i: affine coefficients*, ESAIM: M2AN, 51 (2016), pp. 321–339, https://doi.org/10.1051/m2an/2016045.

[27] A. Cohen and R. DeVore, *Approximation of high-dimensional parametric pdes*, Acta Numerica, 24 (2015), pp. 1–159, https://doi.org/10.1017/S0962492915000033.

[28] A. Cohen, R. DeVore, and C. Schwab, *Analytic regularity and polynomial approximation of parametric and stochastic elliptic pde's*, Analysis and Applications, 09 (2011), pp. 11–47, https://doi.org/10.1142/S0219530511001728.

[29] A. Cohen and G. Migliorati, *Multivariate approximation in downward closed polynomial spaces*, in Contemporary Computational Mathematics - A Celebration of the 80$^{\text{th}}$ Birthday of Ian Sloan, J. Dick, F. Y. Kuo, and H. Woźniakowski, eds., Springer International Publishing, Cham, 2018, pp. 233–282, https://doi.org/10.1007/978-3-319-72456-0_12.

[30] S. Constable, *Ten years of marine csem for hydrocarbon exploration*, Geophysics, 75 (2010), pp. 75A67–75A81, https://doi.org/10.1190/1.3483451.

[31] W. Dahmen, *How to best sample a solution manifold?*, in Sampling Theory, a Renaissance: Compressive Sensing and Other Developments, E. G. Pfander, ed., Springer International Publishing, Cham, 2015, pp. 403–435, https://doi.org/10.1007/978-3-319-19749-4_11.

[32] R. DeVore, G. Petrova, and P. Wojtaszczyk, *Greedy algorithms for reduced bases in banach spaces*, Constructive Approximation, 37 (2013), pp. 455–466, https://doi.org/10.1007/s00365-013-9186-2.

[33] R. A. DeVore, *Chapter 3: The theoretical foundation of reduced basis methods*, in Model Reduction and Approximation, Society for Industrial and Applied Mathematics, jul 2017, pp. 137–168, https://doi.org/10.1137/1.9781611974829.ch3.

[34] J. Dick, F. Y. Kuo, and I. H. Sloan, *High-dimensional integration: The quasi-monte carlo way*, Acta Numerica, 22 (2013), pp. 133–288, https://doi.org/10.1017/S0962492913000044.

[35] O. Ernst, B. Sprungk, and L. Tamellini, *Convergence of sparse collocation for functions of countably many gaussian random variables (with application to elliptic pdes)*, SIAM Journal on Numerical Analysis, 56 (2018), pp. 877–905, https://doi.org/10.1137/17M1123079.

[36] T. Gerstner and M. Griebel, *Dimension–adaptive tensor–product quadrature*, Computing, 71 (2003), pp. 65–87, https://doi.org/10.1007/s00607-003-0015-5.

[37] R. G. Ghanem and P. D. Spanos, *Stochastic Finite Elements: A Spectral Approach*, Springer-Verlag New York, 1991, https://doi.org/10.1007/978-1-4612-3094-6.

[38] M. B. Giles, *Multilevel monte carlo methods*, Acta Numerica, 24 (2015), pp. 259–328, https://doi.org/10.1017/S096249291500001X.

[39] I. Graham, F. Kuo, D. Nuyens, R. Scheichl, and I. Sloan, *Quasi-monte carlo methods for ellip-*

tic PDEs with random coefficients and applications, Journal of Computational Physics, 230 (2011), pp. 3668–3694, https://doi.org/10.1016/j.jcp.2011.01.023.

[40] I. G. Graham, F. Y. Kuo, J. A. Nichols, R. Scheichl, C. Schwab, and I. H. Sloan, *Quasi-monte carlo finite element methods for elliptic pdes with lognormal random coefficients*, Numerische Mathematik, 131 (2015), pp. 329–368, https://doi.org/10.1007/s00211-014-0689-y.

[41] M. D. Gunzburger, C. G. Webster, and G. Zhang, *Stochastic finite element methods for partial differential equations with random input data*, Acta Numerica, 23 (2014), pp. 521–650, https://doi.org/10.1017/S0962492914000075.

[42] B. Haasdonk, K. Urban, and B. Wieland, *Reduced basis methods for parameterized partial differential equations with stochastic influences using the karhunen–loève expansion*, SIAM/ASA Journal on Uncertainty Quantification, 1 (2013), pp. 79–105, https://doi.org/10.1137/120876745.

[43] M. W. Hess and P. Benner, *Fast evaluation of time-harmonic maxwell's equations using the reduced basis method*, IEEE Transactions on Microwave Theory and Techniques, 61 (2013), pp. 2265–2274, https://doi.org/10.1109/TMTT.2013.2258167.

[44] M. W. Hess, S. Grundel, and P. Benner, *Estimating the inf-sup constant in reduced basis methods for time-harmonic maxwell's equations*, IEEE Transactions on Microwave Theory and Techniques, 63 (2015), pp. 3549–3557, https://doi.org/10.1109/TMTT.2015.2473157.

[45] J. S. Hesthaven, G. Rozza, and B. Stamm, *Certified Reduced Basis Methods for Parametrized Partial Differential Equations*, Springer, 2015, https://doi.org/10.1007/978-3-319-22470-1.

[46] J. S. Hesthaven, B. Stamm, and S. Zhang, *Certified reduced basis method for the electric field integral equation*, SIAM Journal on Scientific Computing, 34 (2012), pp. A1777–A1799, https://doi.org/10.1137/110848268.

[47] B. Hosseini, N. Nigam, and J. M. Stockie, *On regularizations of the dirac delta distribution*, Journal of Computational Physics, 305 (2016), pp. 423–447, https://doi.org/10.1016/j.jcp.2015.10.054.

[48] D. Huynh, G. Rozza, S. Sen, and A. Patera, *A successive constraint linear optimization method for lower bounds of parametric coercivity and inf-sup stability constants*, Comptes Rendus Mathematique, 345 (2007), pp. 473–478, https://doi.org/10.1016/j.crma.2007.09.019.

[49] Kirchner, Kristin, Urban, Karsten, and Zeeb, Oliver, *Maxwell's equations for conductors with impedance boundary conditions: Discontinuous galerkin and reduced basis methods*, ESAIM: M2AN, 50 (2016), pp. 1763–1787, https://doi.org/10.1051/m2an/2016006.

[50] A. Kirsch and F. Hettlich, *The Mathematical Theory of Time-Harmonic Maxwell's Equations*, vol. 190, Springer, 2015, https://doi.org/10.1007/978-3-319-11086-8.

[51] G. J. Lord, C. E. Powell, and T. Shardlow, *An Introduction to Computational Stochastic PDEs*, Cambridge University Press, 2014, https://doi.org/10.1017/cbo9781139017329.

[52] A. Manzoni and F. Negri, *Heuristic strategies for the approximation of stability factors in quadratically nonlinear parametrized pdes*, Advances in Computational Mathematics, 41 (2015), pp. 1255–1288, https://doi.org/10.1007/s10444-015-9413-4.

[53] MATLAB, *version 9.0 (R2016a)*, The MathWorks Inc., Natick, Massachusetts, 2016.

[54] P. Monk, *Finite element methods for Maxwell's equations*, Numerical mathematics and scientific computation, Clarendon Press Oxford, Apr. 2003, https://doi.org/10.1093/acprof:oso/9780198508885.001.0001.

[55] F. Nobile, L. Tamellini, F. Tesei, and R. Tempone, *An adaptive sparse grid algorithm for elliptic pdes with lognormal diffusion coefficient*, in Sparse Grids and Applications-Stuttgart 2014, Springer, 2016, pp. 191–220, https://doi.org/10.1007/978-3-319-28262-6_8.

[56] G. D. Prato and J. Zabczyk, *Stochastic Equations in Infinite Dimensions*, Cambridge University Press, 2014, https://doi.org/10.1017/cbo9781107295513.

[57] A. Quarteroni, A. Manzoni, and F. Negri, *Reduced Basis Methods for Partial Differential Equations: An Introduction*, vol. 92, Springer, 2015, https://doi.org/10.1007/978-3-319-15431-2.

[58] M. E. Rognes, R. C. Kirby, and A. Logg, *Efficient assembly of h(div) and h(curl) conforming finite elements*, SIAM Journal on Scientific Computing, 31 (2010), pp. 4130–4151, https://doi.org/10.1137/08073901X.

[59] G. Rozza, D. B. P. Huynh, and A. T. Patera, *Reduced basis approximation and a posteriori error estimation for affinely parametrized elliptic coercive partial differential equations*, Archives of Computational Methods in Engineering, 15 (2008), pp. 229–275, https://doi.org/10.1007/s11831-008-9019-9.

[60] S. A. Sauter and C. Schwab, *Boundary element methods*, Springer, 2011, https://doi.org/10.1007/978-3-540-68093-2_4.

[61] R. Scheichl, A. M. Stuart, and A. L. Teckentrup, *Quasi-monte carlo and multilevel monte carlo methods for computing posterior expectations in elliptic inverse problems*, SIAM/ASA Journal on Uncertainty Quantification, 5 (2017), pp. 493–518, https://doi.org/10.1137/16m1061692.

[62] C. Schillings and C. Schwab, *Sparse, adaptive smolyak quadratures for bayesian inverse problems*, Inverse Problems, 29 (2013), p. 065011, https://doi.org/10.1088/0266-5611/29/6/065011.

[63] C. Schillings and C. Schwab, *Sparsity in bayesian inversion of parametric operator equations*, Inverse Problems, 30 (2014), p. 065007, https://doi.org/10.1088/0266-5611/30/6/065007.

[64] C. Schillings and C. Schwab, *Scaling limits in computational bayesian inversion*, ESAIM: M2AN, 50 (2016), pp. 1825–1856, https://doi.org/10.1051/m2an/2016005.

[65] C. Schwab and A. M. Stuart, *Sparse deterministic approximation of bayesian inverse problems*, Inverse Problems, 28 (2012), p. 045003, https://doi.org/10.1088/0266-5611/28/4/045003.

[66] R. C. Smith, *Uncertainty Quantification: Theory, Implementation, and Applications (Computational Science and Engineering)*, Computational science and engineering, SIAM, 2014.

[67] T. Sullivan, *Introduction to Uncertainty Quantification*, Springer International Publishing, 2015, https://doi.org/10.1007/978-3-319-23395-6.

[68] A. L. Teckentrup, P. Jantsch, C. G. Webster, and M. Gunzburger, *A multilevel stochastic collocation method for partial differential equations with random input data*, SIAM/ASA Journal on Uncertainty Quantification, 3 (2015), pp. 1046–1074, https://doi.org/10.1137/140969002.

[69] H. Widom, *Asymptotic behavior of the eigenvalues of certain integral equations*, Trans. Amer. Math. Soc., 109 (1963), pp. 278–295.

[70] D. Xiu and J. S. Hesthaven, *High-order collocation methods for differential equations with random inputs*, SIAM Journal on Scientific Computing, 27 (2005), pp. 1118–1139, https://doi.org/10.1137/040615201.

[71] D. Xiu and G. E. Karniadakis, *The wiener–askey polynomial chaos for stochastic differential equations*, SIAM Journal on Scientific Computing, 24 (2002), pp. 619–644, https://doi.org/10.1137/s1064827501387826.

[72] L. Zhong, S. Shu, G. Wittum, and J. Xu, *Optimal error estimates for nedelec edge elements for time-harmonic maxwell's equations*, Journal of Computational Mathematics, 27 (2009), pp. 563–572, https://doi.org/10.4208/jcm.2009.27.5.011.